

Accepted Manuscript

Dynamics of deep submarine silicic explosive eruptions in the Kermadec arc, as reflected in pumice vesicularity textures

Melissa D. Rotella, Colin J.N. Wilson, Simon J. Barker, C. Ian Schipper, Ian C. Wright, Richard J. Wysoczanski

PII: S0377-0273(15)00173-0
DOI: doi: [10.1016/j.jvolgeores.2015.05.021](https://doi.org/10.1016/j.jvolgeores.2015.05.021)
Reference: VOLGEO 5556

To appear in: *Journal of Volcanology and Geothermal Research*

Received date: 10 April 2015
Accepted date: 29 May 2015



Please cite this article as: Rotella, Melissa D., Wilson, Colin J.N., Barker, Simon J., Ian Schipper, C., Wright, Ian C., Wysoczanski, Richard J., Dynamics of deep submarine silicic explosive eruptions in the Kermadec arc, as reflected in pumice vesicularity textures, *Journal of Volcanology and Geothermal Research* (2015), doi: [10.1016/j.jvolgeores.2015.05.021](https://doi.org/10.1016/j.jvolgeores.2015.05.021)

This is a PDF file of an unedited manuscript that has been accepted for publication. As a service to our customers we are providing this early version of the manuscript. The manuscript will undergo copyediting, typesetting, and review of the resulting proof before it is published in its final form. Please note that during the production process errors may be discovered which could affect the content, and all legal disclaimers that apply to the journal pertain.

Dynamics of deep submarine silicic explosive eruptions in the Kermadec arc, as reflected in pumice vesicularity textures

Melissa D. Rotella¹, Colin J. N. Wilson¹, Simon J. Barker^{1,2}, C. Ian Schipper¹, Ian C. Wright³, Richard J. Wysoczanski⁴

¹School of Geography, Environment and Earth Sciences
Victoria University of Wellington
P.O. Box 600, Wellington 6140, New Zealand
Email: mrotella@gmail.com
Tel: +64 4 463 9510 Fax: +64 4 463 5418

²School of Environment
University of Auckland
Auckland, New Zealand

³National Oceanography Centre
University of Southampton, Waterfront Campus
Southampton, United Kingdom

⁴National Institute of Water and Atmospheric Research
Wellington, New Zealand

Revised manuscript for: Journal of Volcanology and Geothermal Research

ABSTRACT

Despite increasing recognition of silicic pumice-bearing deposits in the deep marine environment, the processes involved in explosive silicic submarine eruptions remain in question. Here we present data on bubble sizes and number densities (number of bubbles per unit of melt matrix) for deep submarine-erupted pumices from three volcanoes (Healy, Raoul SW and Havre) along the Kermadec arc (SW Pacific) to investigate the effects of a significant (>~1 km) overlying water column and the associated increased hydrostatic pressure on magma vesiculation and fragmentation. We compare these textural data with those from chemically similar, subaerially-erupted pyroclasts from nearby Raoul volcano as well as submarine-erupted 'Tangaroan' fragments derived by non-explosive, buoyant detachment of foaming magma from Macauley volcano, also along the Kermadec arc. Deep submarine-erupted pumices are macroscopically similar (colour, density, texture) to subaerial or shallow submarine-erupted pumices, but show contrasting microscopic bubble textures. Deep submarine-erupted pyroclasts have fewer small (<10 μm diameter) bubbles and narrower bubble size distributions (BSDs) when compared to subaerially erupted pyroclasts from Raoul (35-55 μm vs. 20-70 μm range in volume based median bubble size, respectively). Bubble number density (BND) values are consistently lower than subaerial-erupted pyroclasts and do not display the same trends of decreasing BND with increasing vesicularity. We interpret these textural differences to result from deep submarine eruptions entering the water column at higher pressures than subaerial eruptions entering the atmosphere (~10 MPa vs. 0.1 MPa for a vent at 1000 mbsl). The presence of an overlying water column acts to suppress rapid acceleration of magma, as occurs in the upper conduit of subaerial eruptions, therefore suppressing coalescence, permeability development and gas loss,

amounting to closed-system degassing conditions. The higher confining pressure environment of deep submarine settings hinders extensive post-fragmentation clast expansion, coalescence of bubbles, and thinning of bubble walls, causing clasts to have similar BND values regardless of their vesicularity. Although deep submarine-erupted pyroclasts are closely similar to their subaerial counterparts on the basis of bulk vesicularities and macroscopic appearance, they differ markedly in their microscopic textures, allowing them to be fingerprinted in modern and ancient pumiceous marine sediments.

1. Introduction

Eruptive conditions accompanying voluminous pumice-forming submarine eruptions have been the centre of much study and debate, driven by challenges in observations and documentation (e.g., Fiske and Matsuda, 1964; Burnham, 1983; Cas et al., 1990; Cashman and Fiske, 1991; Fiske et al., 2001; White et al., 2003; Wohletz, 2003; Busby, 2005; Downey and Lentz, 2006). For some time, it was widely accepted that pumice-forming eruptions could not occur under pressures in excess of the critical point of seawater (~2200-3000 m water depth depending on salinity), and were unlikely at >1000 m water depth (e.g., McBirney, 1963; Cas and Wright, 1987; Cas et al., 1990; Cas, 1992). This view has changed in recent years as seafloor exploration has documented an increasing number of deepwater silicic calderas and pumice outcrops, many at depths of >1000 m below sea level (mbsl). Submarine calderas and pumice deposits have now been described from the Izu-Bonin arc (Halbach et al., 1989; Fiske et al., 2001; Yuasa and Kano, 2003; Kutterolf et al., 2014), the Woodlark and eastern Manus basins (Binns, 2003), the southern Mariana arc (Bloomer and Stern, 2001) and along the Tonga-Kermadec arc (Wright et al.,

1998, 2003, 2006; Wright and Gamble, 1999; Barker et al., 2012). In addition, numerical and experimental models have aided the understanding of volatile exsolution processes and indicated that explosive eruptions can theoretically occur at pressures equivalent to water depths of >3 km (Burnham, 1983; Wohletz, 2003; Downey and Lentz, 2006; Stix and Philips, 2012), provided that dissolved volatile contents and discharge rates are sufficiently high.

In the subaerial environment, the dynamics of explosive pumice-forming eruptions are widely documented, with in-situ field studies, eye-witness observations and experimental and theoretical models providing an extensive understanding of eruption processes, from bubble nucleation and vesiculation through to plume dynamics (e.g., Sparks, 1986; Woods, 1988; Cashman and Mangan, 1994; Klug and Cashman, 1994; Sparks et al., 1997; Cichy et al., 2011; Gonnermann and Houghton, 2012). Parallels have not been widely drawn, however, to silicic eruptions in the submarine environment, as many of the relevant parameters are difficult to model and constrain due to: (1) the vastly different conditions and range of unconstrained variables (e.g., multiple phases present, large density contrasts, and processes occurring within the probable range of the critical point of seawater) (e.g., McBirney, 1963; Kano et al., 1996; Wohletz, 2003; Downey and Lentz, 2006; Woods, 2010), and (2) the difficulty of sampling and interpreting deposits in the comparatively inaccessible and grossly under observed submarine environment (e.g., Halbach et al., 1989; Fiske et al., 2001; Hekinian et al., 2008). Therefore, many questions remain about the effect(s) that a large overlying water column has on silicic explosive eruption processes. In this paper we advance the current knowledge of submarine silicic explosive eruptions through a quantitative investigation of vesicularity textures in deep submarine-erupted pumice pyroclasts.

Quantitative 2-D textural studies of subaerial-erupted pyroclasts have provided valuable insights into magma storage, ascent and eruption conditions for silicic explosive eruptions both in natural (e.g., Toramaru, 1990; Klug and Cashman, 1994; Polacci et al., 2001, 2003; Klug et al., 2002; Houghton et al., 2003, 2010; Gurioli et al., 2005; Carey et al., 2009; Giachetti et al., 2010, 2011; Shea et al., 2010; Alfano et al., 2012; Rotella et al., 2013, 2014) and experimentally derived pyroclasts (e.g., Hurwitz and Navon, 1994; Mangan and Sisson, 2000; Mourtada-Bonnefoi and Laporte, 2004; Burgisser and Gardner, 2005; Gardner and Ketcham, 2011). This study uses a similar approach by measuring bubble size and number density characteristics from 2D thin section images. Pyroclast bubble textural data and major element glass chemistry in clasts from three deep submarine volcanoes (Healy, Raoul SW, Havre) are compared to subaerially erupted pyroclastic deposits sampled within stratigraphic intervals from Raoul volcano (Rotella et al., 2014) and submarine-erupted ‘Tangaroan’ pyroclasts dredged from the seafloor around Macauley volcano, which are interpreted to have been generated non-explosively at intermediate eruption rates (Rotella et al., 2013). By comparing and contrasting vesicle textures from each eruptive setting, we show that the presence of a deep overlying water column significantly affects vesiculation processes during eruption and that deep submarine-erupted pumices may be uniquely distinguishable by their vesicle microtextures.

2. Geological setting and sample collection

The Kermadec arc (Fig. 1) results from intra-oceanic subduction of the Pacific plate beneath the Indo-Australian plate to the northeast of New Zealand (Smith and Price, 2006, for overview). The arc consists dominantly of submarine volcanoes, with only Raoul, Macauley, Curtis and L’Esperance volcanoes being partially emergent

(Fig. 1). The occurrence of silicic explosive volcanism along the arc has long been apparent in subaerial deposits (e.g., Brothers and Martin, 1970; Lloyd and Nathan, 1981; Lloyd et al., 1996). However, not until detailed bathymetric mapping and submarine sampling was undertaken was it recognized that submarine caldera-related, silicic explosive volcanism is widespread (e.g., Wright and Gamble, 1999; Haase et al., 2002; Wright et al., 2002, 2003, 2006; Graham et al., 2008). The Kermadec arc volcanoes offer the opportunity to compare and contrast eruptions in the subaerial and deep submarine environments as they have explosively erupted silicic magmas within the last 10 kyr (Lloyd and Nathan, 1981; Lloyd et al., 1996; Worthington et al., 1999; Wright, 2001; Smith et al., 2003a, 2003b, 2006; Wright et al., 2003, 2006; Barker et al., 2012, 2013; Rotella et al., 2014; Carey et al., 2014). Samples for this study were acquired during the 2007 voyage of the R.V. *Tangaroa* (TAN0706) by seafloor dredging at Healy and Raoul SW volcanoes, and by the H.M.N.Z.S. *Canterbury* shipboard crew and scientists on 9 August 2012 from a floating pumice raft which resulted from the 19-20 July eruption of Havre volcano.

2.1. Healy volcano

Healy volcano is a wholly submerged silicic composite volcanic complex consisting of a central edifice with a smaller caldera (1.3 km diameter) at 1150 mbsl on its upper SW flank, and a larger caldera (~2 km diameter) at 1700 mbsl on its NE mid-lower flank (Fig. 2a) (Wright and Gamble, 1999; Barker et al., 2012). Sidescan sonar imagery and dredge sampling shows the volcanic complex is mantled with pumice deposits over an area of >50 km² (Wright and Gamble, 1999; Wright, 2001; Wright et al., 2003). Wright et al. (2003, 2006) suggested that a large recent eruption, to which they attributed 10-15 km³ of pyroclastic material, caused the caldera

collapse. Despite wide variations in clast colours and textures at Healy (Wright et al., 2006), analysed pumices occupy a narrow compositional range (69.5-71.5 wt % SiO₂) in comparison to the broader compositional fields for eruptions sampled within the eruptive stratigraphy on Raoul volcano or dredged from the seafloor around Macauley volcano (Barker et al., 2012, 2013). Textural analyses of samples from three dredge sites along the NW and SE sectors of Healy are used in this study to focus on the most widely dispersed products of the larger explosive event(s) at the volcano. Material sampled closer to the NE/SW trending lineations of ridges and cones that run along the eastern side of the volcanic complex following the caldera rim (Fig. 2a) contained a greater variety of material that plausibly was sourced from multiple eruptions of contrasting styles (Barker et al., 2012).

2.2. Raoul SW volcano

Raoul SW volcano is located ~20 km southwest of Raoul Island (Fig. 1), and was discovered during the TAN0706 voyage of the R.V. *Tangaroa* in 2007 by Kongsberg EM300 multibeam ecosounder mapping (Barker et al., 2012). Raoul SW has a caldera with a diameter of ~4 km and a floor depth of ~1200 mbsl (Fig. 2b). The caldera truncates the summit of an edifice that extends SE beyond the area surveyed in 2007. Samples were acquired by two opportunistic dredges of the caldera rim and floor (Fig. 2b) and consist of exceedingly fresh, highly vesicular pumice. Whole rock analyses showed that these pumices have the most evolved compositions (73.5-75.0 wt. % SiO₂) of the volcanoes in this study (Barker et al., 2012, 2013). The pristine morphology of Raoul SW volcano and the fresh appearance of the pumice suggest that this has been the site of Holocene volcanism (Barker et al., 2012, 2013).

2.3. *Havre volcano*

Havre volcano is a wholly submerged silicic caldera located west of the Kermadec ridge, similar in setting to Healy and Brothers volcanoes to the south (Wright et al., 2006) (Fig. 1). The caldera at Havre truncates a 1 km high edifice and is ~3 km wide with walls rising 540 m above the floor at 1520 mbsl (Fig. 2c). Havre erupted on 19-20 July 2012, emitting an atmospheric steam plume and generating a thermal hot spot observed by MODIS imagery, accompanied by frequent magnitude 3-5 earthquakes between 17-21 July (Carey et al., 2014). A pumice raft was created which within 1 day spread to 400 km² and was dispersed over an area of ~20,000 km² after a further few days (Jutzler et al., 2014). Pre- and post-eruption bathymetry of the volcanic edifice revealed the caldera floor to be >50 m shallower in places, with a bulge on the western caldera wall, and the creation of multiple new vents with depths up to 1400 mbsl as well as several volcanic cones, including one at 640-900 m depth (1.2 km across) on the existing caldera rim (Carey et al., 2014). Based on preliminary volume estimates of the products transported into the raft and those deposited on the seafloor, a bulk erupted volume for the 2012 eruption of at least 1.5 km³ has been proposed (Carey et al., 2014). Our study investigates ~1-4 cm diameter pyroclasts sampled in August 2012 at 30°24'S, 179°27'E from the floating pumice raft ~ 165 km NW of Havre volcano. As pumice from the August 2012 raft is unequivocally from a documented submarine eruption, it is used to compare density, chemistry and textural characteristics with clasts dredged from the seafloor around Healy and Raoul SW volcanoes.

3. Methods

3.1. *Textural quantification*

Densities were determined for 16-32 mm sized pyroclasts dredged from the seafloor deposits around Healy and Raoul SW volcanoes (Barker et al., 2012) as well as rafted pumice from the 2012 Havre eruption (Fig. 3) using the methods of Houghton and Wilson (1989). Densities were then converted to vesicularities assuming a dense rock equivalent (DRE) of 2.4 g/cm^3 (Fig. 3). Polished, impregnated thin sections were made of 37 clasts, spanning the range of measured densities. Of these, 31 representative clasts were imaged for textural analysis and 13 clasts were further selected for quantitative vesicularity measurements of bubble number density (BND) and bubble size distributions (BSD) (Fig. 3). Thin sections were imaged with a flatbed scanner at 3200 dpi, then a series of nested magnification backscattered electron (BSE) images were taken on a JEOL JXA-8320 electron microprobe at Victoria University of Wellington until the smallest bubbles were ≥ 5 pixels in diameter, corresponding to an uncertainty in bubble size measurement of $\leq 5\%$ for one incorrect pixel (Shea et al., 2010). Binary images were created using Adobe Photoshop and bubble number volumes (N_V) were calculated for binned bubble diameters using the FOAMS program with a bubble diameter cut-off size of 5 pixels (Shea et al., 2010). BND values and bubble volume fractions were calculated (Table 1) following the stereological conversion equations of Sahagian and Proussevitch (1998). BND values were corrected for vesicularity and phenocryst content ($>30 \mu\text{m}$ crystals) to avoid underestimating the nucleation densities of highly expanded clasts (after Klug et al., 2002) and to allow direct comparisons between clasts of differing density. BND values in this study can be directly compared to other studies in which the smallest bubbles present were quantified. See Rotella et al. (2014) for a detailed description of the pyroclast imaging and measurement methods used.

Small bubbles (<~30 μm diameter, herein defined as equivalent spherical diameter) have been shown to dominate the number density distributions for silicic subaerial-erupted pumices at Raoul volcano (Rotella et al., 2014). In addition, it has been demonstrated that accurate vesicularity-corrected BND values can be obtained by quantifying bubbles in only the 500x (or 500x and 150x) magnification images (see Rotella et al. (2014) for further details). The same was found to be true for the deep submarine-erupted pyroclasts of this study therefore BND values were obtained using a full suite of magnification images for 8 samples and for an additional 5 samples using only 500x images (Table 1). One caveat in quantifying bubbles in only the highest magnification images is that true volume fraction BSDs cannot be obtained. This is because although the smallest bubbles in pumice are by far the most numerous, the largest bubbles contribute the majority of the volume (Rotella et al., 2014).

3.2. Geochemical analyses

The groundmass glass major element composition was analyzed for each thin section with glass wide enough to place a defocused 10 μm electron beam in order to assess the uniformity of the clast population (Table 2). Glass compositions were measured on the same electron microprobe as used to obtain BSE images, using wavelength dispersive spectrometry (WDS) following the techniques outlined in Barker et al. (2013). Calibrated international standards and secondary standards were analyzed as unknowns throughout the analytical sessions to monitor instrumental drift and precision and accuracy. Approximate 2 SD analytical precisions calculated from repeated analysis of standards are generally <5 relative % for oxides that occur in

concentrations >1 wt. %. Raw data are available on request from the corresponding author.

Whole rock major and trace element analyses were undertaken for two Havre samples for comparison to Healy and Raoul SW (Barker et al., 2013). Whole-rock powders were analysed for major elements by X-ray fluorescence at the Open University, United Kingdom. Approximate 2 standard deviation (2SD) analytical precisions are generally <1-3 relative %. Trace elements were measured on a Thermo Scientific Element2 sector-field ICP-MS at Victoria University of Wellington following the techniques outlined in Barker et al. (2013; Table 3). Approximate 2 SD analytical precisions derived from replicate analyses of a secondary standard (BCR-2) are < 6-7 relative % for most trace elements.

4. Results and interpretation

4.1. Pyroclast vesicularities and sample selection

The density/vesicularity distributions of pyroclasts dredged from the seafloor around Healy and Raoul SW volcanoes (Barker et al. 2012), and from the Havre pumice raft, are broadly similar to those from non-degassed, dry-type subaerial eruptions at Raoul volcano (Rotella et al., 2014), as well as shallow submarine-erupted but subaerial-emplaced Sandy Bay Tephra from Macauley Island (Fig. 3; Barker et al., 2012, their Fig. 11).

At Healy volcano, quantitative textural measurements were made on clasts across the range in vesicularity from one dredge site (D37, Fig. 3a). This site is located 2-3 km from the caldera rim on the NW flank, away from the linear dome-like features on the SE flank (Fig. 2a). The clasts from D37 show similar density/vesicularity distributions to clasts from other dredges at Healy volcano and

Raoul SW volcano as well as those from Raoul Island and submarine-erupted but subaerial emplaced Sandy Bay Tephra on Macauley Island (Barker et al., 2012, their Fig. 11). One modal vesicularity clast from each dredge D36 (distal NW flank) and D46 (distal SE flank) were analysed for comparison to clasts from dredge D37 (Fig. 3b, c). Clasts representing the low vesicularity mode of dredge D46 (SE flank) (Fig. 3c) show a broad range in textures with high microlite and crystal contents and degassed bubble textures (c.f. Klug and Cashman, 1994; Mongrain et al., 2008; Rotella et al., 2014), which may not be attributable to an explosive source and are therefore not the focus of this study. Three clasts from the inner caldera rim dredge (D22) of Raoul SW volcano (Fig. 2b) were chosen for quantitative analysis (Fig. 3d). The 56 Havre pumice raft pyroclasts sampled show a range in vesicularity from 66-89% (Fig. 3e). Due to the limited number of clasts, and potential sampling bias of those which remained afloat one month after the eruption, the density/vesicularity frequency histogram cannot be directly compared to those from dredged pyroclasts. Regardless, there appears to be broad similarities in vesicularity to pyroclasts from Healy and Raoul SW volcanoes with clasts as high as 89% vesicularity (Fig. 3). Thin sections were made across the range in vesicularity and three thin sections were chosen for quantitative analysis (Fig. 3e).

4.2. Qualitative textural results

Despite their similar vesicularities and textural appearances on a macroscopic scale (Barker et al., 2012), deep submarine-erupted pyroclasts have markedly different microtextures than subaerial-erupted pyroclasts from Raoul volcano (e.g., Rotella et al., 2014) or submarine non-explosively erupted Tangaroan pyroclasts from the seafloor around Macauley volcano (Rotella et al., 2013). Deep submarine-erupted

pumices have homogeneous textures with low-vesicularity clasts containing distinctive sub-round or ellipsoidal bubbles with thick (up to 80 μm) walls composed of microlite-free groundmass glass (Fig. 4a, 5). With increasing clast vesicularity the bubbles become larger and increasingly polygonal, with thinning of bubble walls to ~ 1 μm between some adjoining bubbles but still with some thicker (up to ~ 10 μm) bubble walls. Overall there appears to be little evidence for bubble coalescence. In contrast, subaerial-erupted pumices of similar density from Raoul volcano have thin (1-10 μm) bubble walls regardless of clast vesicularity (Fig 4b; Rotella et al., 2014). Low-vesicularity subaerial pumices have a large abundance of small (<10 μm) bubbles dominating the groundmass, and high vesicularity subaerial pumices show evidence for bubble coalescence such as large bubbles with thinned, wrinkled and retracted bubble walls (Klug et al., 2002; Rotella et al., 2014).

Deep submarine-erupted pumices from Healy, Raoul SW and Havre volcanoes have an average phenocryst content of typically $<5\%$ (and not exceeding 15%), dominantly of plagioclase with lesser amounts of clinopyroxene, orthopyroxene, amphibole and Fe-Ti oxides (Barker et al., 2013). The phenocrysts in pumice from all three volcanoes tend to occur both as single crystals and in clusters (Barker et al., 2013) often with a jacket of coarser bubbles within which the crystals are suspended in a cradle of glass films (Fig. 6a-c), herein termed 'palisade' texture (after van den Bogaard and Schmincke, 1986). Phenocrysts are commonly broken in a manner in which they appear to have been pulled apart by tensile forces (Fig. 6c-e) (Giachetti et al., 2010; Miwa and Geshi, 2012) or forced apart by expansion of melt inclusions (Fig. 6f) (Tait, 1992; Best and Christiansen, 1997; Kennedy et al., 2005; Matthews et al., 2012). Crystal fragments are commonly bridged by thin films of glass (Fig. 6d-f) indicating that the crystal split while the magma was still liquid (Best and

Christiansen, 1997; Kennedy et al., 2005; Giachetti et al., 2010; Matthews et al., 2012; Miwa and Geshi, 2012). Bubbles in palisade clusters tend to be larger than groundmass bubbles and often have thicker bubble walls (Fig. 6a-c), and the clusters themselves often appear to have acted as rigid ovoids around which the groundmass glass bubble texture is distorted (Fig. 6a).

Dredged pumice clasts commonly also contain pockets of ingested mud, volcanic ash and foraminifera tests (particularly in Healy and Raoul SW pyroclasts), typically intermingled with the groundmass glass or lining large bubbles within the interiors of large clasts (Fig. 6g,h). Up to 5% of Healy and Raoul SW clasts show light pink oxidation coloration, suggesting that hot clasts ($\sim 800^{\circ}\text{C}$: Tait et al., 1998) met the atmosphere despite 0.5 to >1 km of overlying water column (Barker et al., 2012). Macroscopic bubble textures in pink clasts are not significantly different to those from non-pink clasts suggesting that the pyroclast textures were quenched prior to oxidisation.

4.3. *Quantitative textural results*

The microtextural differences between the deep submarine-erupted pumices and their subaerially-erupted counterparts are reflected in their BSD and BND data. Deep submarine-erupted pyroclasts have fewer small ($<20\ \mu\text{m}$) and large ($>100\ \mu\text{m}$) bubbles, resulting in a well-defined bubble mode of $\sim 45\ \mu\text{m}$ (Figs. 7, 8). Cumulative volume distributions for deep submarine-erupted pyroclasts have steeper slopes compared to subaerially erupted pyroclasts from Raoul volcano, also reflecting the smaller range in bubble sizes (Fig. 8). This is seen in the median bubble size for deep submarine-erupted pyroclasts occurring over a narrower size range ($\sim 35\text{-}55\ \mu\text{m}$) than for subaerial Raoul pyroclasts ($\sim 20\text{-}70\ \mu\text{m}$: Rotella et al., 2014) (Fig. 8).

Deep submarine-erupted pyroclast BSDs also differ from those of non-explosively erupted Tangaroan pyroclast fragments from Macauley volcano (Fig. 9). Tangaroan fragments have strong gradients in vesicularity from ~60 to 90% over distances as short as 2-3 cm, with accompanying gradients in BSDs and BND values indicative of complex growth histories (Rotella et al., 2013). Deep submarine-erupted pyroclasts, however, show little variation in BSDs for clasts of a comparable range in vesicularity (~70-90%) (Fig. 9).

The ranges in BND values for deep submarine-erupted pyroclasts in this study are also markedly different to those for subaerial-erupted Raoul pyroclasts of similar vesicularity (Fig. 10). Raoul pyroclasts show BND values that are linked to clast vesicularity, with clasts that quenched closest to the moment of fragmentation preserving the highest BND values (up to $1.9 \times 10^{10} \text{ cm}^{-3}$) and clasts with higher vesicularities containing lower BND values (as low as $2.6 \times 10^9 \text{ cm}^{-3}$), reflecting syn- and post-fragmentation expansion and coalescence of bubbles (Rotella et al., 2014). Deep submarine-erupted pyroclasts, however, have overall much lower BND values ($6.0 \times 10^8 - 1.9 \times 10^9 \text{ cm}^{-3}$) and do not show discernable variations in BND with clast vesicularity (Fig. 10). Deep submarine-erupted pyroclasts in turn have BND values significantly higher than for across the vesicularity range within a single Tangaroan type clast ($8.8 \times 10^7 - 4.8 \times 10^8 \text{ cm}^{-3}$; Rotella et al., 2013). These differences imply the presence of contrasting eruption dynamics for deep submarine explosive eruptions (Fig. 9).

4.4. Geochemical results

Healy, Raoul SW and Havre pumice glasses are rhyodacite to rhyolite in composition (72.5-79 wt% SiO₂) and yield a homogeneous and compositionally

distinctive chemical suite for each volcano (Fig. 11; Table 2), consistent with the whole rock chemistry data of Barker et al. (2012, 2013). The chemical homogeneity shown by pyroclasts sampled at different dredge sites rules out the possibility of contrasting magma sources contributing to the pyroclast population, as seen for seafloor pyroclast fragments from Macauley volcano (Barker et al., 2012; Rotella et al., 2013). The chemistry of the deep submarine-erupted pyroclasts are distinctive for their position along the arc, which is consistent with other studies of Kermadec arc pyroclasts (e.g., Gamble et al., 1993, 1995, 1996; Smith et al., 2003a, 2003b; Wright et al., 2006; Barker et al., 2013). The distinctive low-K chemistry of the most northern volcanoes (Raoul and Raoul SW) further rules out sampling of these pyroclasts in dredge hauls from Macauley and Healy. Interestingly, the major element glass chemistry of July 2012 Havre raft pumice is nearly indistinguishable from that of Healy pumice, with the only discernable difference being lower chlorine content (Fig. 11). Havre raft pumices, however, are distinctive from Healy pumices in their whole rock trace element chemistry with significantly different concentrations many element including Sr, Ba, Cs and Pb (Table 3). Pumices from the July 2012 Havre raft have markedly similar whole rock major and trace element chemistry to older dredged Havre pumices sampled by Wright et al. (2006) (Table 3).

5. Discussion

Deep submarine-erupted pyroclasts have significantly different microtextures, BSD patterns and BND values to subaerial-erupted pyroclasts (Raoul: Rotella et al., 2014; Mt Mazama: Klug et al., 2002; and Mt St Helens: Klug and Cashman, 1994) as well as submarine-erupted Tangaroan pyroclasts (Rotella et al., 2013) implying that the dynamics of deep submarine explosive silicic eruptions differ in some key

respects. Below, we consider what might cause these differences and propose a first-order conceptual eruption model for deep submarine eruptions.

5.1. Deep submarine explosive silicic eruptions: physical considerations

Without the ability to witness deep submarine explosive silicic eruptions, generalised inferences must be made as to what eruption variables are affected by the presence of a deep overlying water column. Fewer theoretical models exist for submarine pumice eruptions (e.g., Kano et al., 1996; Cashman and Fiske, 2001; Downey and Lentz, 2006; Allen and McPhie 2009; Woods, 2010) compared to the wealth of observational data and resulting models for subaerial pumice eruptions (e.g., Wilson et al., 1980; Sparks, 1986; Woods, 1988, 1995, 2010; Mastin, 2002; Mangan et al., 2004a, 2004b; Mastin et al., 2009; Ogden, 2011; Saffaraval et al., 2012). For example, Mastin et al. (2009) outline model source parameters (such as eruption column height and grain size) for ten styles of subaerial eruption but no parameters exist for eruptions occurring in >50 m water depth. Gum rosin-acetone analogue experiments have implied that given sufficient volatile content (4-6 wt.% H₂O) and rapid decompression and volatile exsolution, subaqueously erupted magma can explosively fragment in water depths corresponding to pressures greater than the critical point of seawater (~3000 mbsl) (Stix and Philips, 2012). The role of water (vs. air) in submarine eruptions, as reviewed by White et al. (2003), is recognized to largely affect steam generation, pressure, heat capacity and magma rheology in the eruption dynamics, yet direct relation to eruption processes are not made. In comparison to air, water is a denser, more viscous and relatively incompressible fluid and therefore the pressures (static and dynamic) exerted on the eruption jet and plume are significantly higher in deep submarine eruptions than for subaerial eruptions, as

long as the erupting mixture of gas, liquid and pyroclasts does not puncture the surface of the ocean and temporarily revert to pressures closer to atmospheric. In turn, pyroclasts are likely to experience less pressure differential between the stages of fragmentation and eventual quenching (i.e., cooling of the clast below the glass transition temperature), mostly due to the hydrostatic pressure of the water column.

5.2. Using bubble size distributions to interpret vesiculation processes in deep submarine eruptions

Theoretical models and textural studies of subaerially-erupted pyroclasts highlight a critical vesicularity range of 65-75% beyond which further vesiculation is considered to be restricted by mutual interference of bubbles (Sparks, 1978; Gardner et al., 1996; Rust and Cashman, 2011; Rotella et al., 2014). This is illustrated in pyroclast density/vesicularity distributions from Raoul volcano (Rotella et al., 2014), where there is a dearth of pyroclasts within this vesicularity range, with dominant vesicularity modes of ~82% resulting from syn- and post-fragmentation expansion. In addition, BND values for Raoul pyroclasts are greatest for pyroclasts near the critical vesicularity range and decrease with increasing vesicularity, which is also interpreted to reflect permeability development and continued bubble coalescence and growth after fragmentation but before quenching (Fig. 10). Deep submarine-erupted pyroclasts have similar density/vesicularity distributions to subaerial-erupted Raoul pyroclasts (Barker et al., 2012, their Fig. 11; Rotella et al., 2012) (Fig. 3). However, deep marine-erupted pumices do not mirror the high BND values near the critical vesicularity range seen in the Raoul pyroclasts, nor do they have decreasing BND values with increasing vesicularity (Table 1, Fig. 10).

Bubble nucleation rates (and hence BND values) have been numerically proposed, and experimentally demonstrated, to increase with decompression rate in silicic magmas (Toramaru, 1990, 1995, 2006; Hurwitz and Navon, 1994; Mangan and Sisson, 2000; Mangan et al., 2004a; Mourtada-Bonnefoi and Laporte, 2004; Massol and Koyaguchi, 2005; Hamada et al., 2010; Cichy et al., 2011; Gardner and Ketcham, 2011; Gonnermann and Gardner, 2013). A correlation between BND values and eruption vigour is shown for subaerially-erupted clasts from Raoul volcano (Rotella et al., 2014), but has not been investigated in submarine settings. We postulate that although deep submarine-erupted pyroclasts would undergo similar fragmentation processes as their counterparts in subaerial eruptions, they would experience less overall decompression as they enter the higher-pressure environment of deep water versus the atmosphere. This higher-pressure environment would inhibit ‘run-away’ bubble nucleation (Cashman and Mangan, 1994) and would instead favour extended periods of bubble growth prior to interaction with water and quenching, resulting in overall lower BND values when compared to similar sized eruptions in the subaerial environment.

Evidence of a bubble growth-dominated regime for deep submarine-erupted pyroclasts, as opposed to a coalescence-dominated regime for subaerial-erupted pyroclasts, can be seen in a flat to mildly increasing trend of BND with vesicularity (Fig. 10), as predicted by Herd and Pinkerton (1997). A growth-dominated bubble regime is also evident from bubble size distributions (Fig. 12, Table 1) (Blower et al., 2002; Gaonac’h et al., 1996a, 1996b, 2003; Gonnermann and Manga, 2007). Exponential bubble-size distributions are widely interpreted to reflect bubble nucleation and viscosity-limited diffusional bubble growth (e.g., Toramaru, 1995; Navon et al., 1998; Liu and Zhang, 2000; Lensky et al., 2004), whereas power law

distributions are considered to represent bubble coalescence (e.g., Gaonac'h et al., 1996a, 1996b, 2003; Lovejoy et al., 2004) or extended intervals of continued nucleation (Blower et al., 2002). Pyroclasts from deep submarine-erupted volcanoes yield bubble size patterns that closely approximate exponential distributions for bubbles up to $\sim 80 \mu\text{m}$, with an overlap in the fit of exponential and power law models for bubbles between ~ 20 and $\sim 80 \mu\text{m}$, and bubbles $> \sim 80 \mu\text{m}$ fitting power law distributions (Fig. 12a, Table 1). In addition, curves for low and high-vesicularity clasts from Healy volcano are parallel with an apparent shift to larger bubble sizes with increasing vesicularity, indicative of a bubble growth dominated regime. This observation is in contrast to that seen in bubble populations from subaerial-erupted Raoul pyroclasts which fit exponential distributions for bubbles up to $\sim 20 \mu\text{m}$ for low-vesicularity pyroclasts and $\sim 50 \mu\text{m}$ for high vesicularity pyroclasts (Fig. 12b). Also, unlike the Healy curves, Raoul low- and high-vesicularity pyroclast curves cross at $\sim 7 \mu\text{m}$, indicating an increase in larger bubbles at the expense of smaller bubbles, indicative of coalescence (Fig 12b). The smallest bubbles in size distributions are proposed to represent the last few nucleation events in a continuously nucleating system and larger bubbles to reflect the earliest formed bubbles that have undergone varying histories of growth and coalescence, as seen in the experiments of Namiki et al. (2003) and modeled by Massol and Koyaguchi (2005). The extension of the exponential law distribution for bubbles from $20 \mu\text{m}$ to $> 80 \mu\text{m}$ (Fig. 12a), therefore, implies an increased growth and nucleation regime for deep submarine-erupted pyroclasts compared to their subaerial counterparts.

5.3. Vesiculation and fragmentation dynamics for deep submarine explosive silicic eruptions

Given the distinct vesicularity textures of the deep submarine-erupted pumices associated with their eruption setting, we consider the possible effects that an overlying water column would have on the vesiculation and fragmentation dynamics. Below we adopt a first order approach in applying basic quantitative limits to processes which could be occurring at different eruptive stages and hypothesize what could be driving the differences in pyroclast textures. Healy volcano is used as a working example, but similar inferences could be made for Havre and Raoul SW given their similar magma chemistries, calculated intensive parameters (e.g., Barker et al., 2013) and similar pyroclast textures.

5.3.1. Pre-eruptive magma conditions

Previous studies of Healy volcano allow pre-eruptive conditions to be quantified. Barker et al. (2013) used Fe-Ti oxide thermometry to calculate pre-eruptive magma temperatures of $\sim 850^{\circ}\text{C}$. Amphibole hygrometry (Barker et al., 2013) and melt inclusion analyses (Saunders, 2009) indicate magmatic H_2O contents of 4.5-5 wt. %. Using the amphibole thermobarometry pressure calculations of Ridolfi et al. (2010), Barker et al. (2013) also estimated the Healy magma chamber to be at a pressure of 100 – 150 MPa prior to eruption, equivalent to 3.5 – 5.3 km depth within the oceanic crust (assuming no overlying water column and crustal density of 2.89 g/cm^3). Wright et al. (2003) suggested that prior to the caldera forming eruption at Healy a pre-eruptive caldera edifice may have existed between depths of 550 - 1000 mbsl. Using these edifice reconstruction depths, the pressure of the overlying water column equates to 5.6 – 10.2 MPa pressure (seawater density of 1.035 g/cm^3), equivalent to 200 – 360 m of overlying oceanic crust, which is notably small compared to the pressure difference between magma chamber and vent and less than the variation in

pressures given by amphibole barometry. Here we adopt the conservative pre-eruptive edifice reconstruction depth of 1000 m (Wright et al., 2003) and intermediate magma chamber pressure of 125 MPa (Barker et al., 2013) which would place the magma chamber at ~4 km depth below the reconstructed edifice (Fig. 13) typical of Kermadec Arc magma chamber depths (Wysoczanski et al., 2012). Based on the determined magma temperature and volatile contents, the rhyolite magma is calculated to be volatile saturated at magma chamber pressures of >160 MPa (Newman and Lowenstern, 2002). This is supported by the presence of palisade bubble textures (Fig. 7) indicating that the magma may have experienced early bubble formation at significant depths prior to eruption.

5.3.2. Bubble nucleation and fragmentation

Bubble nucleation has been numerically and experimentally demonstrated to be largely driven by pressure differentials experienced by volatile-rich magmas during rapid decompression (e.g., Sparks, 1978; Toramaru, 2006; Stix and Phillips, 2012). Bubble nucleation occurs when supersaturation is sufficient for large nucleation rates, defined by Hurwitz and Navon (1994) to occur at supersaturation pressures of 10 to >70 MPa, depending on the sites available for heterogeneous nucleation. The more volatile-rich the magma is, the shallower in the conduit bubbles can continue to nucleate if large supersaturations are present. With the extra pressure (~10 MPa) of a 1000 m water column at Healy, the level at which bubble nucleation and fragmentation occurred would be shifted ~360 metres shallower relative to the vent in comparison to if the eruption were occurring in a subaerial environment. In addition, the Healy magma would have experienced a smaller pressure drop on fragmentation, due to the pressure of the overlying water column, and therefore undergone less

vigorous nucleation just prior to fragmentation. As a first order approach, assuming the same eruptive conditions as the May 1980 Mt St. Helens dacite, in which fragmentation is shown to have occurred 520 m below the subaerial vent (13.8 MPa assuming overlying rock density of 2.7 g/cm^3 : Klug and Cashman, 1994), the Healy fragmentation zone would have been ~ 130 m below the submarine vent (Fig. 13a).

5.3.3. *The gas thrust region and convective plume*

Plinian subaerial silicic explosive eruptions have peak eruption intensities that range from $1.6 \times 10^6 - 1.1 \times 10^9 \text{ kg/s}$, with most around $10^7 - 10^8 \text{ kg/s}$ (e.g., Carey and Sigurdsson, 1989) and the basal gas thrust region (or jet) is powered by its initial momentum with negligible buoyancy effects (Sparks, 1986). For dry-type subaerial eruptions, jet heights can reach from 0.5 to 4 km above the vent, but this figure varies with magma temperature and gas content, exit velocity and vent radius (Woods, 1988). The rising jet decelerates as the initial kinetic energy is expended, and the bulk density of the mixture decreases from entrainment and heating of the surrounding air. It is unknown, however, to what distances the gas thrust region can penetrate in the submarine environment, but it will decelerate more rapidly than its subaerial counterparts due to the higher confining pressure, decreased momentum through ingestion of a higher density medium, and rapid cooling by water (e.g., Cashman and Fiske, 1991; Koyaguchi and Woods, 1996). Some studies have postulated the gas thrust region to reach 200-400 m (e.g., the Yali and Filakopi Pumice Breccias: Kano et al., 1996) but this distance has not been quantified.

In subaerial eruptions, the convective plume region occurs when the initial kinetic energy of the gas thrust region is expended and upward buoyancy due to entrainment and heating of the atmosphere takes over (Woods, 1988). In the

submarine environment, however, the strong confining dynamic pressure, coupled with the higher density and dynamic viscosity, and efficient cooling capability of the ambient seawater would condense the steam in the plume and act to prevent the formation of a buoyant gas/particle plume as in subaerial eruptions. Instead, the 'plume' is envisaged to occur as a heated water + pyroclast mixture that may or may not rise buoyantly (Kano et al., 1996; Allen and McPhie, 2009). The dynamics of the submarine plume are thus predicted to be divorced from the jet region and are not envisaged to affect the jet.

If the hot steam-filled pyroclasts come in contact with cold seawater or seafloor sediments the pyroclasts would cool rapidly and the magmatic steam in bubbles within the pyroclasts would condense and create a vacuum in which seawater and sediments would be sucked in (e.g. Allen et al., 2008). Evidence of this is seen in the abundance of benthic and planktonic forams, volcanic ash and mud that is present deep in the interior of some pyroclasts from Healy (Fig. 6g, h).

5.3.4. Submarine eruption dynamics and evidence for closed system degassing

Our findings imply that although deep submarine-erupted magmas achieve vesicularities of 90% or more, the pressure of the overlying water column acts to suppress permeability development via bubble coalescence, which results in limited outgassing before quenching of the pyroclasts. The initial phases of the eruption, in which a large amount of energy is released by exsolving volatiles, would see the volcanic jet penetrate into the overlying water column with little regard for the higher pressure submarine environment when compared to that of the atmosphere (Fig. 13a). Bubble nucleation and fragmentation is inferred to occur within the conduit as for subaerial eruptions, albeit at shallower conduit levels than if the eruption occurred at

atmospheric pressure. An overlying 1000 m water column exerting 10 MPa pressure at vent, however, would hinder the rapid acceleration of magma in the upper conduit typically experienced by subaerial eruptions as the magma approaches atmospheric pressure from ~10 MPa (Castro et al., 2012) (Fig. 14a). The lack of rapid acceleration in the submarine realm would also lead to less extreme bubble coalescence caused by shearing (Okumura et al., 2009).

Deep submarine-erupted pyroclast porosities provide evidence for eruptions occurring under equilibrium degassing conditions. The porosities of Healy, Raoul SW and Havre pyroclasts coincide with the equilibrium magma porosity of ~75% predicted by Burgisser and Gardner (2005) at 10 MPa, the pressure at vent (Fig. 14b). In comparison pyroclasts erupted at atmospheric pressure have porosities that are not in agreement with equilibrium degassing conditions, and these pyroclasts are interpreted to have undergone permeable outgassing prior to quenching (e.g., Rust and Cashman, 2011). Further increases in deep submarine-erupted pyroclast vesicularities from 75% to their final quenched values would be attained through bubble growth in the subaqueous eruption jet (Fig. 10, 13). This interpretation is supported by the lack of qualitative and quantitative evidence for large-scale coalescence in pumice textures (Figs. 4a, 5) and bubble number and size distributions (Figs. 7, 8, 10 and 12).

With increasing jet vigour (i.e., increasing height in the water column and hence a reduction in the overlying pressure) the fragmentation zone may propagate deeper into the conduit in response to the reduced confining pressure (Fig. 13b). This is inferred to cause the gas-rich magma (supersaturated, as evidenced by the palisade bubble textures: Fig. 6) to rapidly decompress and fragment, and cause the adhering pre-existing bubbles on crystals to rapidly expand and pull apart the crystals (Fig. 6c-e). At 1000 mbsl, the penetration of the jet into the water column could reduce the

effective confining pressure in the conduit, causing the nucleation and fragmentation zone to deepen. Due to the density and high heat capacity per unit volume of seawater, and its high inertia (exerting a dynamic pressure) acting to decelerate the jet, the jet may episodically condense and collapse or shrink, resulting in an increase in the confining pressure that acts back down into the conduit, causing the fragmentation surface to rise again (Fig. 13c). These processes are likely to happen cyclically within a sustained explosive eruption event, similar to the pulses witnessed during the submarine basaltic eruption of NW Rota-1 volcano, Mariana arc, (Deardorff et al., 2011) albeit on a much larger scale and over longer time periods.

5.4. What happens if/when the jet breaches the sea surface?

At a depth of 1000 mbsl, as for Healy volcano, the eruption jet would most likely be contained within the water column, but might periodically breach the sea surface. The presence of pink oxidized clasts making up $\sim < 5\%$ of the Healy (and Raoul SW) pyroclast population was taken by Barker et al. (2012) to infer that the pyroclasts met air while still hot (~ 800 °C, cf. Tait et al., 1998). Since the textures of these pyroclasts are not significantly different to non-pink Healy and Raoul SW pyroclasts with similar BND values and BSDs we infer that the clast texture was quenched-in before the jet breached the water-atmosphere interface. However, as shown in this study, the gradual build-up of the submarine jet, and lowering of the fragmentation level, could provide the right conditions for the jet to penetrate the water column periodically.

If the eruption jet breaches the sea surface while the pyroclasts are still above the glass transition temperature, such as would be the case for powerful eruptions in shallower water, then an additional sudden decrease in pressure would be experienced by the pyroclasts and an additional nucleation event could occur. Such may be the

case for the 6.3 C¹⁴ka Sandy Bay Tephra eruption of Macauley volcano, which erupted through ~400 m of water and emplaced up to 100 m of cross-bedded, non-welded, poorly stratified dacite ignimbrite, as seen on the 3 km² subaerial exposure of the volcano's eastern flank (Lloyd et al., 1996; Barker et al., 2012). The Sandy Bay eruption is interpreted to have interacted extensively with water, given the evidence for cool emplacement of ignimbrite on Macauley Island such as lack of oxidation coloration, ubiquitous ash coatings on pumice pyroclasts and lack of a pyroclastic fall deposit. The Sandy Bay Tephra ignimbrite shows field evidence for syn-eruptive mixing with water and wet emplacement as the ashy matrix is frequently vesicular and preserves irregular hollows, inferred to represent water or steam trapped during deposition (Barker et al., 2012), similar to textures in the phreatoplinian Hatepe ash from the 232 AD eruption of Taupo, New Zealand (Wilson and Walker, 1985; Smith and Houghton, 1995) and phase three of the Minoan eruption of Santorini (Sparks and Wilson, 1990). The Sandy Bay Tephra pumices have similar density spectra to deep submarine-erupted pyroclasts (Barker et al., 2012, their Fig. 11); however, the microtextures are markedly different with a higher degree of heterogeneity both within individual pyroclasts and between pyroclasts (Fig. 15), which precluded meaningful 2D quantitative analyses of bubble size and number densities. The Sandy Bay Tephra pyroclast bubbles appear similar to Raoul subaerially erupted pyroclasts (thinned and contorted bubble walls with high degrees of coalescence) but often contain extensive regions of small micron-scale bubbles, which occur as ribbons and pockets throughout the clasts, sometimes between regions of larger bubbles (Fig. 15a). We attribute the pockets of numerous small bubbles to a late-stage nucleation event that occurred when the submarine eruption jet breached the sea surface and transitioned to a subaerial eruption plume with an associated sudden drop in pressure.

Similar numerous small bubbles were seen to form within the first 10 seconds bubble growth in the 4D X-ray microtomographic experiments of Baker et al. (2012) before quickly coalescing into a foam of larger bubbles.

The textures of Sandy Bay Tephra pyroclasts indicate that shallow water, highly explosive eruptions may reflect a hybrid eruption regime between those of deep submarine and subaerial settings. As suggested for Tangaroan style submarine eruptions (Rotella et al., 2013), there is likely a spectrum of explosive submarine eruption styles, with significantly changing conditions possible within individual eruptions resulting from variable pressure regimes at different water depths and/or eruption vigour. Notably, the distinctive conditions associated with deep submarine eruptions yield pyroclasts with textures that are measurably distinctive from their subaerial counterparts, opening up the possibility of fingerprinting deep submarine-erupted pyroclasts in modern or ancient pumice-bearing marine sediments.

6. Conclusions

Deep submarine-erupted silicic pyroclasts from the Kermadec arc have distinctive vesicularity textures compared to subaerially erupted pyroclasts from nearby Raoul volcano, with fewer small bubbles ($<10\ \mu\text{m}$) and a narrower (volume based) median vesicle size of $35\text{-}55\ \mu\text{m}$ (compared to $20\text{-}70\ \mu\text{m}$). In addition, deep submarine-erupted pyroclasts show overall lower BND values with relatively consistent BND values with increasing vesicularity, owing to a bubble growth dominated regime compared to a coalescence dominated regime for subaerial-erupted Raoul pumices. We attribute these observations to the higher-pressure regime in deep submarine eruptions, where the lower pressure drop at vent in the deep submarine environment, compared to eruptions which occur into atmosphere, would result in less

potential for bubble nucleation, causing overall lower BND values. The higher-pressure confining environment of the deep ocean hinders the ability for the bubbles in the fragmented magma to undergo drastic amounts of expansion as they would in atmosphere. Suppressed expansion results in reduced bubble wall thinning and bubble coalescence and the magma does not experience significant permeability development and consequent gas loss (outgassing). Shallow erupted Sandy Bay Tephra pyroclasts, however, show that when the jet breaches the water atmosphere interface, the sudden pressure drop promotes late stage nucleation of bubbles resulting in highly heterogeneous textures with pockets of small numerous bubbles. The wide range of variables affecting submarine eruption dynamics and plume stability means that a wide range of outcomes and eruption models are possible with differing water depths and eruptive rates. Although similar in their macroscopic appearance, subaerial- and deep submarine-erupted pyroclasts record markedly contrasting eruptive conditions in their microtextures, opening up the possibility of fingerprinting pyroclast origins in the marine record.

Acknowledgements We thank the Master and crew of the R.V. *Tangaroa* on the TAN07/06 (2007) voyage for their logistical support. The New Zealand Department of Conservation gave permission for the fieldwork on Macauley Island in 2007, and Max Borella, Darren Gravley and Mike Rosenberg helped with shipboard and field studies. Helen Bostock and the shipboard party of the August 2012 voyage of the H.M.N.Z.S. *Canterbury* are acknowledged for the Havre floated pumice raft samples. Lucia Gurioli, Ben Kennedy and John Townend are thanked for helpful discussions and Lionel Wilson is gratefully thanked for his editorial handling. This research was supported by a Royal Society of New Zealand through a Marsden Fund Grant

(VUW0613) awarded to CJNW and ICW and a James Cook Research Fellowship awarded to CJNW.

ACCEPTED MANUSCRIPT

References

- Alfano, F., Bonadonna, C., Gurioli, L., 2012. Insights into eruption dynamics from textural analysis: The case of the May, 2008, Chaiten eruption. *Bulletin of Volcanology* 74, 2095-2108.
- Allen, S.R., McPhie, J., 2009. Products of neptunian eruptions. *Geology* 37, 639-642.
- Allen, S.R., Fiske, R.S., Cashman, K.V., 2008. Quenching of steam-charged pumice: Implications for submarine pyroclastic volcanism. *Earth and Planetary Science Letters* 274, 40-49.
- Baker, D.R., Mancini, L., Polacci, M., Higgins, M.D., Gualda, G.A.R., Hill, R.J., Rivers, M.L., 2012. An introduction to the application of X-ray microtomography to the three-dimensional study of igneous rocks. *Lithos* 148, 262-276.
- Barker, S.J., Rotella, M.D., Wilson, C.J.N., Wright, I.C., Wysoczanski, R.J., 2012. Contrasting pyroclast density spectra from subaerial and submarine silicic eruptions in the Kermadec arc: Implications for eruption processes and dredge sampling. *Bulletin of Volcanology* 74, 1425-1443.
- Barker, S.J., Wilson, C.J.N., Baker, J.A., Millet, M-A., Rotella, M.D., Wright, I.C., Wysoczanski, R.J., 2013. Geochemistry and petrogenesis of silicic magmas in the intra-oceanic Kermadec arc. *Journal of Petrology* 54, 351-391.
- Best, M.G., Christenson, E.H., 1997. Origin of broken phenocrysts in ash-flow tuffs. *Geological Society of America Bulletin* 109, 63-73.
- Binns, R.A., 2003. Deep marine pumice from the Woodlark and Manus Basins, Papua New Guinea. In: White, J.D.L., Smellie, J.L., Clague, D.A., (Eds.), *Explosive subaqueous volcanism*. American Geophysical Union, *Geophysical Monograph* 140, 329-343

- Bloomer, S.H., Stern, R.J., 2001. Mantle inputs to the subduction factory: Detailed study of the southern Mariana seamount province. *EOS, Transactions AGU* 82, 47.
- Blower, J.D., Keating, J.P., Mader, H.M., Phillips, J.C., 2002. The evolution of bubble size distributions in volcanic eruptions. *Journal of Volcanology and Geothermal Research* 120, 1-23.
- Brothers, R.N., Martin, K.R., 1970. The geology of Macauley Island, Kermadec Group, Southwest Pacific. *Bulletin Volcanologique* 34, 330-346.
- Burgisser, A., Gardner, J.E., 2005. Experimental constraints on degassing and permeability in volcanic conduit flow. *Bulletin of Volcanology* 67, 42-56.
- Burnham, C.W., 1983. Deep submarine pyroclastic eruptions. *Economic Geology Monograph* 5, 142-148.
- Busby, C., 2005. Possible distinguishing characteristics of very deepwater explosive and effusive silicic volcanism. *Geology* 33, 845-848.
- Carey, R.J., Houghton, B.F., Thordarson, T., 2009. Abrupt shifts between wet and dry phases of the 1875 eruption of Askja Volcano: Microscopic evidence for macroscopic dynamics. *Journal of Volcanology and Geothermal Research* 184, 256-270.
- Carey, R.J., Wysoczanski, R., Wunderman, R., Jutzeler, M., 2014. Discovery of the largest historic silicic submarine eruption. *EOS, Transactions AGU* 95, 157-159.
- Carey, S.N., Sigurdsson, H., 1989. The intensity of plinian eruptions. *Bulletin of Volcanology* 51, 28-40.

- Cas, R.A.F., 1992. Submarine volcanism: Eruption styles, products, and relevance to understanding the host-rock successions to volcanic-hosted massive sulfide deposits. *Economic Geology* 87, 511-541.
- Cas, R.A.F., Wright, J.V., 1987. *Volcanic Successions, modern and ancient*. London, Allen and Unwin, 528 pp.
- Cas, R.A.F., Allen, R.L., Bull, S.W., Clifford, B.A., Wright, J.V., 1990. Subaqueous, rhyolitic dome-top tuff cones: A model based on the Devonian Bunga Beds, southeastern Australia and a modern analogue. *Bulletin of Volcanology* 52, 159-174.
- Cashman, K.V., Fiske, R.S., 1991. Fallout of pyroclastic debris from submarine volcanic eruptions. *Science* 253, 275-280.
- Cashman, K.V., Mangan, M.T., 1994. Physical aspects of magmatic degassing II. Constraints on vesiculation processes from textural studies of eruptive products. *Reviews in Mineralogy* 30, 447-478.
- Castro, J.M., Burgisser, A., Schipper, C.I., Mancini, S., 2012. Mechanisms of bubble coalescence in silicic magmas. *Bulletin of Volcanology* 74, 2339-2352.
- Cichy, S.B., Botcharnikov, R.E., Holtz, F., Behrens, H. 2011. Vesiculation and microlite crystallization induced by decompression: A case study of the 1991-1995 Mt Unzen eruption (Japan). *Journal of Petrology* 52, 1469-1492.
- Deardorff, N.D., Cashman, K.V., Chadwick Jr., W.W., 2011. Observations of eruptive plume dynamics and pyroclastic deposits from submarine explosive eruptions at NW Rota-1, Mariana arc. *Journal of Volcanology and Geothermal Research* 202, 47-59.
- Downey, W.S., Lentz, D.R., 2006. Modelling of deep submarine pyroclastic volcanism: A review and new results. *Geoscience Canada* 33, 5-24.

- Eichelberger, J.C., Carrigan, C.R., Westrich, H.R., Price, R.H., 1986. Non-explosive silicic volcanism. *Nature* 323, 598-602.
- Fiske, R.S., Matsuda, T., 1964. Submarine equivalents of ash flows in the Tokiwa Formation, Japan. *American Journal of Science* 262, 76-106.
- Fiske, R.S., Naka, J., Iizasa, K., Yuasa, M., Klaus, A., 2001. Submarine silicic caldera at the front of the Izu-Bonin arc, Japan: Voluminous seafloor eruptions of rhyolitic pumice. *Geological Society of America Bulletin* 113, 813-824.
- Gamble, J.A., Wright, I.C., Baker, J.A., 1993. Seafloor geology and petrology in the oceanic to continental transition zone of the Kermadec-Havre-Taupo Volcanic Zone arc system, New Zealand. *New Zealand Journal of Geology and Geophysics* 36, 417-435.
- Gamble, J.A., Wright, I.C., Woodhead, J.D., McCulloch, M.T., 1995. Arc and back-arc geochemistry in the southern Kermadec arc-Ngatoro Basin and offshore Taupo Volcanic Zone, SW Pacific. In: Smellie, J.L. (Ed.), *Volcanism associated with extension at consuming plate margins*. Geological Society of London Special Publications 81, 193-212.
- Gamble, J.A., Woodhead, J.D., Wright, I.C., Smith, I.E.M., 1996. Basalt and sediment geochemistry and magma petrogenesis in a transect from oceanic island arc to rifted continental margin arc: The Kermadec-Hikurangi margin, SW Pacific. *Journal of Petrology* 37, 1523-1546.
- Gaonac'h, H., Lovejoy, S., Stix, J., Schertzer, D., 1996a. A scaling growth model for bubbles in basaltic lava flows. *Earth and Planetary Science Letters* 139, 395-409.

- Gaonac'h, H., Stix, J.B., Lovejoy, S., 1996b. Scaling effects on vesicle shape, size and heterogeneity of lavas from Mount Etna. *Journal of Volcanology and Geothermal Research* 74, 131-153.
- Gaonac'h, H., Lovejoy, S., Schertzer, D. 2003. Percolating magmas and explosive volcanism. *Geophysical Research Letters* 30, 1559.
- Gardner, J.E., Ketcham, R.A., 2011. Bubble nucleation in rhyolite and dacite melts: Temperature dependence of surface tension. *Contributions to Mineralogy and Petrology* 162, 929-943.
- Gardner, J.E., Thomas, R.M.E., Jaupart, C., Tait, S., 1996. Fragmentation of magma during Plinian volcanic eruptions. *Bulletin of Volcanology* 58, 144-162.
- Giachetti, T., Druitt, T.H., Burgisser, A., Arbaret, L., Glaven, C., 2010. Bubble nucleation, growth and coalescence during the 1997 Vulcanian explosions of Soufriere Hills Volcano, Montserrat. *Journal of Volcanology and Geothermal Research* 193, 215-231.
- Giachetti, T., Burgisser, A., Arbaret, L., Druitt, T.H., Kelfoun, K., 2011. Quantitative textural analysis of Vulcanian pyroclasts (Montserrat) using multi-scale X-ray computed microtomography: Comparison with results from 2D image analysis. *Bulletin of Volcanology* 73, 1295-1309.
- Gill, J.B., 1981. *Orogenic andesites and plate tectonics*. Springer: Berlin
- Gonnermann, H.M., Manga, M., 2007. The fluid mechanics inside a volcano. *Annual Review of Fluid Mechanics* 39, 321-356.
- Gonnermann, H.M., Houghton, B.F., 2012. Magma degassing during the Plinian eruption of Novarupta, Alaska, 1912. *Geochemistry, Geophysics, Geosystems* 13, Q10009.

- Gonnermann, H., Gardner, J.E., 2013. Homogeneous bubble nucleation in rhyolitic melt: Experiments and nonclassical theory. *Geochemistry, Geophysics, Geosystems* 14, 4758-4773.
- Graham, I.J., Reyes, A.G., Wright, I.C., Peckett, K.M., Smith, I.E.M., Arculus, R.J., 2008. Structure and petrology of newly discovered volcanic centers in the northern Kermadec-southern Tofua arc, South Pacific Ocean. *Journal of Geophysical Research* 113, B08S02.
- Gurioli, L., Houghton, B.F., Cashman, K.V., Cioni, R., 2005. Complex changes in eruption dynamics during the 79 AD eruption of Vesuvius. *Bulletin of Volcanology* 67, 144-159.
- Haase, K.M., Worthington, T.J., Stoffers, P., Garbe-Schonberg, D., Wright, I., 2002. Mantle dynamics, element recycling, and magma genesis beneath the Kermadec Arc-Havre Trough. *Geochemistry, Geophysics, Geosystems* 3, 1071.
- Halbach, P., Nakamura, K., Wahsner, M., Lange, J., Sakai, H., Kaselitz, L., Hansen, R-D., Yamono, M., Post, J., Prause, B., Seifert, R., Michaelis, W., Teichmann, F., Kinoshita, M., Marten, A., Ishibashi, J., Czerwinski, S., Blum, S., 1989. Probable modern analogue of Kuroko-type massive sulphide deposits in the Okinawa Trough back-arc basin. *Nature* 338, 496-499.
- Hamada, M., Laporte, D., Cluzel, N., Koga, K.T., Kawamoto, T., 2010. Simulating bubble number density of rhyolitic pumices from Plinian eruptions: Constraints from fast decompression experiments. *Bulletin of Volcanology* 72, 735-746.
- Hekinian, R., Mühe, R., Worthington, T.J., Stoffers, P., 2008. Geology of a submarine volcanic caldera in the Tonga Arc: Dive results. *Journal of Volcanology and Geothermal Research* 176, 571-582.

- Herd, R.A., Pinkerton, H., 1997. Bubble coalescence in basaltic lava: Its impact on the evolution of bubble populations. *Journal of Volcanology and Geothermal Research* 75, 137-157.
- Houghton, B.F., Wilson, C.J.N., 1989. A vesicularity index for pyroclastic deposits. *Bulletin of Volcanology* 51, 451-462.
- Houghton, B.F., Hobden, B.J., Cashman, K.V., Wilson, C.J.N., Smith, R.T., 2003. Large-scale interaction of lake water and rhyolitic magma during the 1.8 ka Taupo eruption, New Zealand. In: White, J.D.L., Smellie, J.L., Clague, D.A., (Eds.), *Explosive subaqueous volcanism*. American Geophysical Union, *Geophysical Monograph* 140, 97-109.
- Houghton, B.F., Carey, R.J., Cashman, K.V., Wilson, C.J.N., Hobden, B.J., Hammer, J.E., 2010. Diverse patterns of ascent, degassing, and eruption of rhyolite magma during the 1.8 ka Taupo eruption, New Zealand: Evidence from clast vesicularity. *Journal of Volcanology and Geothermal Research* 195, 31-47.
- Hurwitz, S., Navon, O., 1994. Bubble nucleation in rhyolitic melts: Experiments at high pressure, temperature, and water content. *Earth and Planetary Science Letters* 122, 267-280.
- Jutzler, M., Marsh, R., Carey, R.J., White, J.D.L., 2014. On the fate of pumice rafts formed during the 2012 Havre submarine eruption. *Nature Communications* 5, 3660.
- Kano, K., Tamamoto, T., Ono, K., 1996. Subaqueous eruption and emplacement of the Shinjima Pumice, Shinjima (Moeshima) Island, Kagoshima Bay, SW Japan. *Journal of Volcanology and Geothermal Research* 71, 187-206.
- Kennedy, B., Spieler, O., Scheu, B., Kueppers, U., Taddeucci, J., 2005. Conduit implosion during Vulcanian eruptions. *Geology* 33, 581-584.

- Klug, C., Cashman, K.V., 1994. Vesiculation of May 18, 1980, Mount St. Helens magma. *Geology* 22, 468-472.
- Klug, C., Cashman, K.V., Bacon, C.R., 2002. Structure and physical characteristics of pumice from the climactic eruption of Mount Mazama (Crater Lake), Oregon. *Bulletin of Volcanology* 64, 486-501.
- Koyaguchi, T., Woods, A.W., 1996. On the formation of eruption columns following explosive mixing of magma and surface water. *Journal of Geophysical Research* 101, 5561-5574.
- Kutterolf, S., Schindlbeck, J.C., Scudder, R.P., Murray, R.W., Pickering, K.T., Freundt, A., Labanieh, S., Heydolph, K., Saito, S., Naruse, H., Underwood, M.B., Wu, H., 2014. Large volume submarine ignimbrites in the Shikoku Basin: An example for explosive volcanism in the Western Pacific during the Late Miocene. *Geochemistry, Geophysics, Geosystems* 15, 1837-1851.
- Le Maitre, R.W. (Editor), 1989. A classification of igneous rocks and glossary of terms: Recommendations of the International Union of Geological Sciences, Subcommittee on the Systematics of Igneous Rocks. Blackwell, Oxford, 193 pp.
- Lensky, N.G., Navon, O., Lyakhovskiy, V., 2004. Bubble growth during decompression of magma: experimental and theoretical investigation. *Journal of Volcanology and Geothermal Research* 129, 7-22.
- Liu, Y., Zhang, Y., 2000. Bubble growth in rhyolitic melt. *Earth and Planetary Science Letters* 181, 251-264.
- Lloyd, E.F., Nathan, S. 1981. Geology and tephrochronology of Raoul Island, Kermadec Group, New Zealand. *New Zealand Geological Survey Bulletin* 95, 105 pp.

- Lloyd, E.F., Nathan, S., Smith, I.E.M., Stewart, R.B., 1996. Volcanic history of Macauley Island, Kermadec Ridge, New Zealand. *New Zealand Journal of Geology and Geophysics* 39, 295-308.
- Lovejoy, S., Gaonac'h, H., Schertzer, D., 2004. Bubble distributions and dynamics: The expansion-coalescence equation. *Journal of Geophysical Research* 109, B11203.
- Mangan, M.T., Sisson, T., 2000. Delayed, disequilibrium degassing in rhyolite magma: Decompression experiments and implications for explosive volcanism. *Earth and Planetary Science Letters* 183, 441-455.
- Mangan, M.T., Sisson, T., Hankins, W.B., 2004a. Decompression experiments identify kinetic controls on explosive silicic eruptions. *Geophysical Research Letters* 31, L08605.
- Mangan, M.T., Mastin, L.G., Sisson, T., 2004b. Gas evolution in eruptive conduits: Combining insights from high temperature and pressure decompression experiments with steady-state flow modeling. *Journal of Volcanology and Geothermal Research* 129, 23-36.
- Massol, H., Koyaguchi, T., 2005. The effect of magma flow on nucleation of gas bubbles in a volcanic conduit. *Journal of Volcanology and Geothermal Research* 143, 69-88.
- Mastin, L.G., 2002. Insights into volcanic conduit flow from an open-source numerical model. *Geochemistry, Geophysics, Geosystems* 3, 1037.
- Mastin, L.G., Guffanti, M., Servranckx, R., Webley, P., Barsotti, S., Dean, K., Durant, A., Ewert, J.W., Neri, A., Rose, W.I., Schneider, D., Siebert, L., Stunder, B., Swanson, G., Tupper, A., Volentik, A., Waythomas, C.P., 2009. A multidisciplinary effort to assign realistic source parameters to models of

- volcanic ash-cloud transport and dispersion during eruptions. *Journal of Volcanology and Geothermal Research* 186, 10-21.
- Matthews, N.E., Pyle, D.M., Smith, V.C., Wilson, C.J.N., Huber, C., von Hinsberg, V., 2012. Quartz zoning and the pre-eruptive evolution of the ~340-ka Whakamaru magma systems, New Zealand. *Contributions to Mineralogy and Petrology* 163, 87-107.
- McBirney, A.R., 1963. Factors governing the nature of submarine volcanism. *Bulletin Volcanologique* 26, 455-469.
- Miwa, T., Geshi, N., 2012. Decompression rate of magma at fragmentation: Inference from broken crystals in pumice of vulcanian eruption. *Journal of Volcanology and Geothermal Research* 227-228, 76-84.
- Mongrain, J., Larsen, J.F., King, P.L., 2008. Rapid water exsolution, degassing and bubble collapse observed experimentally in K-phonolite melts. *Journal of Volcanology and Geothermal Research* 173, 178-184.
- Mourtada-Bonnefoi, C.C., Laporte, D., 2004. Kinetics of bubble nucleation in a rhyolitic melt: An experimental study of the effect of ascent rate. *Earth and Planetary Science Letters* 218, 521-537.
- Namiki, A., Hatakeyama, T., Toramaru, A., Kurita, K., Sumita, I., 2003. Bubble size distributions in a convecting layer. *Geophysical Research Letters* 30, 1784.
- Navon, O., Chekhmir, A., Lyakhovsky, V., 1998. Bubble growth in highly viscous melts: Theory, experiments, and autoexplosivity of dome lavas. *Earth and Planetary Science Letters* 160, 763-776.
- Newman, S., Lowenstern, J.B., 2002. VolatileCalc: a silicate melt-H₂O-CO₂ solution model written in Visual Basic for Excel. *Computers and Geoscience* 28, 597-604.

- Ogden, D.E., 2011. Fluid dynamics in explosive volcanic vents and craters. *Earth and Planetary Science Letters* 312, 401-410.
- Okumura, S., Nakamura, M., Takeuchi, S., Tsuchiyama, A., 2009. Magma deformation may include non-explosive volcanism via degassing through bubble networks. *Earth and Planetary Science Letters* 281, 267-274.
- Polacci, M., Papale, P., Rosi, M., 2001. Textural heterogeneities in pumice from the climactic eruption of Mount Pinatubo, 15 June 1991, and implications for magma ascent dynamics. *Bulletin of Volcanology* 63, 83-97.
- Polacci, M., Pioli, L., Rosi, M., 2003. The Plinian phase of the Campanian Ignimbrite eruption (Phlegrean Fields, Italy): Evidence from density measurement and textural characterization of pumice. *Bulletin of Volcanology* 65, 418-432.
- Ridolfi, R., Renzulli, A., Puerini, M., 2010. Stability and chemical equilibrium of amphibole in calc-alkaline magmas: An overview, new thermobarometric formulations and applications to subduction-related volcanoes. *Contributions to Mineralogy and Petrology* 160, 45-66.
- Rotella, M.D., Wilson, C.J.N., Barker, S.J., Wright, I.C., 2013. Highly vesicular pumice generated by buoyant detachment of magma in subaqueous volcanism. *Nature Geoscience* 6, 129-132.
- Rotella, M.D., Wilson, C.J.N., Barker, S.J., Cashman, K.V., Houghton, B.F., Wright, I.C., 2014. Bubble development in explosive silicic eruptions: insights from pyroclast vesicularity textures from Raoul volcano (Kermadec arc). *Bulletin of Volcanology* 76, 826.
- Rust, A.C., Cashman, K.V., 2011. Permeability controls on expansion and size distributions of pyroclasts. *Journal of Geophysical Research* 116, B11202.

- Saffaraval, F., Solovitz, S.A., Ogden, D.E., Mastin, L.G., 2012. Impact of reduced near-field entrainment of overpressured volcanic jets on plume development. *Journal of Geophysical Research* 117, B05209.
- Sahagian, D.L., Proussevitch, A.A., 1998. 3D particle size distributions from 2D observations: Stereology for natural applications. *Journal of Volcanology and Geothermal Research* 84, 173-196.
- Saunders, K.E., 2009. Micro-analytical studies of the petrogenesis of silicic arc magmas in the Taupo Volcanic Zone and southern Kermadec Arc, New Zealand. PhD thesis, Victoria University of Wellington.
- Shea, T., Houghton, B.F., Gurioli, L., Cashman, K.V., Hammer, J.E., Hobden, B.J., 2010. Textural studies of vesicles in volcanic rocks: An integrated methodology. *Journal of Volcanology and Geothermal Research* 190, 271-289.
- Smith, I.E.M., Price, R.C., 2006. The Tonga-Kermadec arc and Havre-Lau back-arc system: Their role in the development of tectonic and magmatic models for the western Pacific. *Journal of Volcanology and Geothermal Research* 156, 315-331.
- Smith, I.E.M., Worthington, T.J., Stewart, R.B., Price, R.C., Gamble, J.A., 2003a. Felsic volcanism in the Kermadec arc, SW Pacific: Crustal recycling in an oceanic setting. In: Larter, R.D., Leat, P.T. (Eds.) *Intra-oceanic subduction systems: Tectonic and magmatic processes*. Geological Society of London Special Publications 213, 99-118.
- Smith, I.E.M., Stewart, R.B., Price, R.C., 2003b. The petrology of a large intra-oceanic silicic eruption: The Sandy Bay Tephra, Kermadec Arc, Southwest Pacific. *Journal of Volcanology and Geothermal Research* 124, 173-194.

- Smith, I.E.M., Worthington, T.J., Price, R.C., Stewart, R.B., Maas, R., 2006. Petrogenesis of dacite in an oceanic subduction environment: Raoul Island, Kermadec arc. *Journal of Volcanology and Geothermal Research* 156, 252-265.
- Smith, R.T., Houghton, B.F., 1995. Vent migration and changing eruptive style during the 1800a Taupo eruption: New evidence from the Hatepe and Rotongaio phreatoplinian ashes. *Bulletin of Volcanology* 57, 432-439.
- Sparks, R.S.J., 1978. The dynamics of bubble formation and growth in magmas: A review and analysis. *Journal of Volcanology and Geothermal Research* 3, 1-37.
- Sparks, R.S.J., 1986. The dimensions and dynamics of volcanic eruption columns. *Bulletin of Volcanology* 48, 3-15.
- Sparks, R.S.J., Wilson, C.J.N., 1990. The Minoan deposits: a review of their characteristics and interpretation. In: Hardy, D.A., Keller, J., Galanopoulos, V.P., Flemming, N.C., Druitt, T.H., (Eds.) *Thera and the Aegean World III*. London: The Thera Foundation, Vol. 2, pp 89-99.
- Sparks, R.S.J., Bursik, M.I., Carey, S.N., Gilbert, J.S., Glaze, L., Sigurdsson, H., Woods, A.W., 1997. *Volcanic plumes*. John Wiley, Hoboken, N.J., 574pp.
- Stix, J., Phillips, J.C., 2012. An analog investigation of magma fragmentation and degassing: Effects of pressure, volatile content, and decompression rate. *Journal of Volcanology and Geothermal Research* 211-212, 12-23.
- Tait, S., 1992. Selective preservation of melt inclusions in igneous phenocrysts. *American Mineralogist* 77, 146-155.
- Tait, S., Thomas, R., Gardner, J., Jaupart, C., 1998. Constraints on cooling rates and permeabilities of pumice in an explosive eruption jet from colour and magnetic mineralogy. *Journal of Volcanology and Geothermal Research* 86, 79-91.

- Toramaru, A., 1990. Measurement of bubble size distributions in vesiculated rocks with implications for quantitative estimation of eruption processes. *Journal of Volcanology and Geothermal Research* 43, 71-90.
- Toramaru, A., 1995. Numerical study of nucleation and growth of bubbles in viscous magmas. *Journal of Geophysical Research* 100, 1913-1931.
- Toramaru, A., 2006. BND (bubble number density) decompression rate meter for explosive volcanic eruptions. *Journal of Volcanology and Geothermal Research* 154, 303-316.
- van den Bogaard, P., Schmincke, H.-U., 1986. Pyroclast morphology and vesicle fabric from magmatic and phreatomagmatic eruptions of Laacher See volcano (Eifel, West Germany). *International Volcanological Congress, Hamilton, New Zealand, 1-9 February 1986, Abstracts*, p. 125.
- White, J.D.L., Smellie, J.L., Clague, D.A., 2003. Introduction: A deductive outline and topical overview of subaqueous explosive volcanism. In: White, J.D.L., Smellie, J.L., Clague, D.A. (Eds.), *Explosive subaqueous volcanism*. American Geophysical Union, *Geophysical Monograph* 140, 1-23.
- Wilson, C.J.N., Walker, G.P.L., 1985. The Taupo eruption, New Zealand I. General aspects. *Philosophical Transactions of the Royal Society of London* A314, 199-228.
- Wilson, L., Sparks, R.S.J., Walker, G.P.L., 1980. Explosive volcanic eruptions - IV. The control of magma properties and conduit geometry on eruption column behaviour. *Geophysical Journal of the Royal Astronomical Society* 63, 117-148.
- Wohletz, K.H., 2003. Water/magma interaction: Physical considerations for the deep submarine environment. In: White, J.D.L., Smellie, J.L., Clague, D.A., (Eds.),

- Explosive subaqueous volcanism. American Geophysical Union, Geophysical Monograph 140, 25-49.
- Woods, A.W., 1988. The fluid dynamics and thermodynamics of eruption columns. *Bulletin of Volcanology* 50, 169-193.
- Woods, A.W., 1995. The dynamics of explosive volcanic eruptions. *Reviews of Geophysics* 33, 495-530.
- Woods, A.W., 2010. Turbulent plumes in nature. *Annual Review of Fluid Mechanics* 42, 391-412.
- Worthington, T.J., Gregory, M.R., Bondarenko, V., 1999. The Denham Caldera on Raoul Volcano: Dacite volcanism in the Tonga-Kermadec arc. *Journal of Volcanology and Geothermal Research* 90, 29-48.
- Wright, I.C., 2001. In situ modification of modern submarine hyaloclastic/pyroclastic deposits by ocean currents: An example from the Southern Kermadec arc (SW Pacific). *Marine Geology* 172, 287-307.
- Wright, I.C., Gamble, J.A., 1999. Southern Kermadec submarine caldera arc volcanoes (SW Pacific): Caldera formation by effusive and pyroclastic eruption. *Marine Geology* 161, 207-227.
- Wright, I.C., de Ronde, C., Faure, K., Gamble, J.A., 1998. Discovery of hydrothermal sulfide mineralization from southern Kermadec arc volcanoes (SW Pacific). *Earth and Planetary Science Letters* 164, 335-343.
- Wright, I.C., Stoffers, P., Hannington, M., de Ronde, C.E.J., Herzig, P., Smith, I.E.M., Browne, P.R.L., 2002. Towed-camera investigations of shallow-intermediate water-depth submarine stratovolcanoes of the southern Kermadec arc, New Zealand. *Marine Geology* 185, 207-218.

- Wright, I.C., Gamble, J.A., Shane, P.A.R., 2003. Submarine silicic volcanism of the Healy caldera, southern Kermadec arc (SW Pacific): I - volcanology and eruption mechanisms. *Bulletin of Volcanology* 65, 15-29.
- Wright, I.C., Worthington, T.J., Gamble, J.A., 2006. New multibeam mapping and geochemistry of the 30°-35° S sector, and overview, of southern Kermadec arc volcanism. *Journal of Volcanology and Geothermal Research* 149, 263-296.
- Wysoczanski, R.J., Handler, M.R., Schipper, C.I., Leybourne, M.I., Creech, J., Rotella, M.D., Nichols, A.R.L., Wilson, C.J.N., Stewart, R.B., 2012. The tectonic source of ore metals and volatile elements in the southern Kermadec arc. *Economic Geology* 107, 1539-1556.
- Yuasa, M., Kano, K., 2003. Submarine silicic calderas on the northern Shichito-Iwojima Ridge, Izu-Ogasawara (Bonin) arc, Western Pacific. In: White, J.D.L., Smellie, J.L., Clague, D.A., (Eds.), *Explosive subaqueous volcanism*. American Geophysical Union, *Geophysical Monograph* 140, 231-243.

Figure Captions

Fig. 1. Regional tectonic setting of the Kermadec arc resulting from the subduction of the Pacific plate under the Indo-Australian plate. Dark grey triangles represent basaltic-andesite volcanoes and light grey circles represent silicic caldera volcanoes. Volcanoes investigated in this study are in bold. Modified from Barker et al. (2012).

Fig. 2. Seafloor bathymetry and sample dredge locations for (a) Healy, (b) Raoul SW and (c) Havre volcanoes from EM300 multibeam mapping. White regions are areas without multibeam data. All bathymetry maps are shown with the same depth scale. Dredge locations are shown by grey lines and labeled by dredge number. Dredge locations for pyroclasts used in this study are marked with an asterisk. Red and blue dotted outlines in (b) depict Raoul and Denham calderas, respectively, and are modified from Worthington et al. (1999). Bathymetry for Healy and Raoul SW volcanoes is from Barker et al. (2012); bathymetry for Havre volcano was collected prior to the July 2012 eruption.

Fig. 3. Density/vesicularity histograms for dredged 16-32 mm clasts from (a-c) Healy, (d) Raoul SW and (e) rafted pumice from the July 2012 eruption of Havre. The red dashed line represents the average density of pumice from subaerial, dry-type eruptions from Raoul volcano (from Rotella et al., 2014). Stars show where representative samples were chosen for textural analysis. White stars are clasts for which thin sections were made and backscattered electron images were taken but bubble textures not quantified; red stars are samples in which bubble textures were quantified. Stars are labelled with the sample number. n indicates the number of

density measurements made. Healy and Raoul SW density data is from Barker et al. (2012). See Fig. 2a,b for Healy and Raoul SW dredge locations.

Fig. 4. Representative BSE images for (a) Healy deep submarine-erupted pyroclasts (Fig. 3a) compared to (b) Raoul subaerial-erupted pyroclasts (Rotella et al., 2014) across the range of densities sampled. Images have been adjusted using Adobe Photoshop so that vesicles are black, glass is white and crystals are grey. ρ is clast density, and BND is the vesicularity corrected bubble number density value. BND values for samples marked with an asterisk were calculated from 500x magnification images only (see text for details). Note the change in scale to 100x magnification for one Raoul sample.

Fig. 5. Representative BSE images for (a) Raoul SW (Fig. 3d) and (b) Havre (Fig. 3e) deep submarine-erupted pyroclasts across the range of densities sampled. Images adjustments and symbol definitions as per Fig 4.

Fig. 6. Representative bubble and crystal textures for submarine-erupted pyroclasts in this study. (a-c) Examples of palisade texture where crystals or crystal clusters are enclosed in a jacket of coarser bubbles. Palisade texture is seen in pyroclasts from all Kermadec volcanoes studied. (c-e) Crystals split parallel to the *c*-axis possibly due to tensile stresses. Note the bridging glass films (solid arrows in c, d, e) indicating that crystals split while the magma was still liquid. Some crystals contain radiating stretched groundmass bubbles which grade into the groundmass bubble texture (d), whereas palisade bubbles can deform groundmass bubbles (a, and dotted arrows in c, f). (g) Representative BSE image of ingested mud, volcanic ash and foraminifera tests

within large bubbles inside some Healy deep submarine-erupted pyroclasts. The volcanic glass shards contain heterogeneous compositions including some basaltic shards. (h) Centre of a decimetre-sized Healy pyroclast exposed by cutting with a rock saw showing ingested material. Scales in the photographs (a) and (h) are in millimetres and centimetres, respectively, and scales for BSE images (b-g) are shown for each.

Fig. 7. BSDs for deep submarine-erupted pyroclasts from Healy, Raoul SW and Havre volcanoes plotted (a) on a linear scale to highlight the large bubble size variations and to emphasise the bubble size modes, and (b) on a log scale to highlight small bubble size variations. Grey field represents data from 14 dry-type non-degassed explosive subaerial eruptions from Raoul volcano spanning the 82% vesicularity mode (Rotella et al., 2014). Density is in g/cm^3 , and the dashed vertical lines mark $30 \mu\text{m}$, the typical subaerial Raoul modal bubble size, for reference. Solid lines are for Healy, dotted line is for Raoul SW, and dashed line is for Havre pyroclasts. Note that the deep submarine-erupted pyroclasts have fewer both small bubbles ($<20 \mu\text{m}$) and larger bubbles ($>100 \mu\text{m}$) when compared to subaerial-erupted Raoul clasts but share a similar modal bubble size.

Fig. 8. Bubble volume distributions for deep submarine-erupted pyroclasts plotted as cumulative volume $<$ vesicle diameter L . Grey field represents data from 14 dry-type non-degassed subaerial eruptions from Raoul (Rotella et al., 2014). Density is g/cm^3 , and the dashed vertical line marks $30 \mu\text{m}$, the typical subaerial Raoul modal bubble size, for reference. The intersection of the curves with the line at 0.5 cumulative volume fraction denotes the volume-based median bubble size. Steeper curves are

indicative of smaller ranges in bubble sizes. Note the comparative scarcity of bubbles smaller than 10 μm , and the steeper slopes and larger median bubble sizes for deep submarine-erupted pyroclasts compared to subaerial-erupted Raoul pyroclasts.

Fig. 9. Comparison of BSDs for deep submarine-erupted pyroclasts from Healy, Raoul SW and Havre volcanoes (blue field) to Tangaroan non-explosively erupted pyroclasts from the seafloor around Macauley volcano (colored lines) from Rotella et al (2013). The Tangaroan data are for four regions across the vesicularity gradient of a single 16-32 mm pyroclast (see Rotella et al., 2013, for further details). Subaerial-erupted pyroclasts from Raoul volcano (grey field) are shown for reference (Rotella et al. 2014). All BSD data are corrected for vesicle and phenocryst areas. Raoul data are for clasts spanning the 82% vesicularity mode, dotted line marks 30 μm , the typical Raoul modal bubble size, for reference.

Fig. 10. Phenocryst- and vesicle-corrected bubble number density (BND) values versus density (lower axis) and vesicularity (upper axis) for Kermadec arc silicic pyroclasts. Data in the blue field are for deep submarine-erupted pyroclasts (Healy, Raoul SW and Havre volcanoes), and data in the grey field are for subaerial-erupted pyroclasts from Raoul volcano (Rotella et al., 2014). Also shown are data for four regions across the vesicularity gradient of a single submarine-erupted Tangaroan pyroclast from Macauley volcano (Rotella et al., 2013). Differing colored symbols for Raoul pyroclasts represent stratigraphically controlled samples from different eruptions, spanning the 82% vesicularity mode (see Rotella et al., 2014, for further details). Dashed black line at 82% vesicularity marks the modal vesicularity of dry-erupted Raoul pyroclasts. Inset depicts theoretical vesiculation trends generated via

nucleation (N), growth (G), coalescence (C) and vesicle loss (L), modified from Herd and Pinkerton (1997). If no error bars are shown then uncertainty is less than the size of the symbol. Uncertainties in density measurements (and hence vesicularity-corrected BND values) are from Barker et al. (2012).

Fig. 11. Major element glass compositions of pyroclasts from deep submarine-erupted Healy, Raoul SW and Havre volcanoes and shallow-erupted Sandy Bay Tephra pyroclasts from Macauley Island. Solid, dotted, and dashed grey fields depict glass data from Barker et al. (2013) for Healy, Raoul SW and the Sandy Bay Tephra (SBT), respectively. Data have been normalized to 100% on a volatile free basis. Low- and medium-K discriminant boundary marked by dashed line on K_2O vs. SiO_2 is from Gill (1981); compositional boundary marked by dashed black line on total alkali (Na_2O+K_2O) vs. SiO_2 is from Le Maitre (1989). Healy pyroclasts are from dredges D36 (dark grey), D37 (black), D44 (white), and D46 (light grey). Standard deviations (SD) are calculated from repeated analysis of glass standards.

Fig. 12. Variation in BND values for representative low and high-vesicularity clasts erupted from the (a) deep submarine environment of Healy volcano and (b) subaerial environment of Raoul volcano (Rotella et al., 2014), where the total number of bubbles larger than a given size ($N_{v>L}$) is shown as a function of bubble size (L). Bubble number volumes (N_v) are corrected for clast vesicularity and phenocryst content. Small bubbles follow exponential distributions (in blue), corresponding to bubble nucleation and diffusional growth, and larger bubbles follow power law distributions (in red), dominated by bubble coalescence. Black symbols represent bubble sizes that fit both an exponential and power law distribution. (a) For deep

submarine-erupted pyroclasts the exponential and power law distributions follow sub-parallel trends with overlap between exponential and power laws (grey zone) over a large range of bubble sizes (~ 23 and $93 \mu\text{m}$) for clasts across the range in vesicularity (Table 1). (b) For subaerial-erupted Raoul pyroclasts the exponential distributions for the low and high vesicularity clasts cross at small bubble sizes with overlap between exponential and power law distributions over a smaller range in bubble sizes for high vesicularity clasts (~ 23 and $50 \mu\text{m}$) and no overlap (dashed arrow) for low vesicularity clasts. Exponential distributions that extend to larger bubble sizes, and hence overlap with power law distributions, are indicative of higher degrees of diffusional growth, potentially through higher degrees of clast expansion (see text and Rotella et al., 2014, for discussion).

Fig. 13. Schematic model illustrating the overall model derived here for deep submarine eruption dynamics. Panels are not to scale, but representative dimensions and figures are added. Magma chamber depth is determined by amphibole thermobarometry (Barker et al., 2013) using the method of Ridolfi et al. (2010). Water depth is assumed from the conservative estimate for pre-caldera edifice reconstruction of Wright et al. (2003). The density of seawater is assumed to be 1.035 g/cm^3 and density of oceanic crust to be 2.89 g/cm^3 (from Ridolfi et al., 2010). In panel (a) the eruption begins in much the same way as it would subaerially with the bubble nucleation and fragmentation zones shifted to shallow levels by only $\sim 360 \text{ m}$ relative to the vent outlet due to the added pressure of the overlying seawater. In panel (b) rise of the eruption jet decreases the pressure experienced within the conduit and nucleation and fragmentation zones deepen. In panel (c) the decelerating and

condensing jet would cause pressure to increase back down into the conduit causing a shallowing of the fragmentation and nucleation zones.

Fig 14. Pressure versus (a) time and (b) porosity for Healy volcano magma under closed system degassing conditions. (a) Curves showing the pressure–time paths of viscous magmas undergoing fast decompression under closed-system degassing for Plinian (solid curves) and sub-Plinian (dashed curves) eruption styles. Coalescence by inter bubble-film planar stretching (green curves) occurs over similar timescales as decompression durations (black curves) (Castro et al., 2012). Note the rapid acceleration of magma, shown as kinks at 10 MPa, attributed to the magma experiencing the effects of atmospheric pressure. For Healy volcano the eruption enters the water column at ~10 MPa (1 km water depth) suppressing rapid acceleration and the resulting extensive coalescence that occurs in the shallowest reaches of subaerial conduits. (b) Red line is the equilibrium porosity from Burgisser and Gardner (2005) for 100 MPa, the minimum magma storage depth determined by amphibole barometry (Barker et al., 2013). Pressure at vent (P_{vent}) is assumed from the pre-caldera edifice reconstruction of Wright et al. (2003). See Fig 14 for other details. At the pressure of fragmentation (P_{frag}) the equilibrium magma porosity is ~65%, and upon eruption the equilibrium magma porosity is ~75%, consistent with predictions of Sparks (1978), Eichelberger et al. (1986) and Rotella et al. (2014).

Fig. 15. Representative BSE images highlighting the textural heterogeneity in a single Sandy Bay Tephra pyroclast. (a) shows a region of numerous small bubbles with thicker groundmass glass and (b) a shows a region of large bubbles with thin bubble

walls. White boxes in 40x images show where the 150x magnification images (at right) were taken.

Table 1. Vesicularity data for Healy, Raoul SW and Havre pyroclasts.

Table 2. Average major element glass concentrations for Healy, Raoul SW and Havre pyroclasts analysed by electron microprobe.

Table 3. Representative major and trace element whole-rock compositions of Kermadec pumices.

ACCEPTED MANUSCRIPT

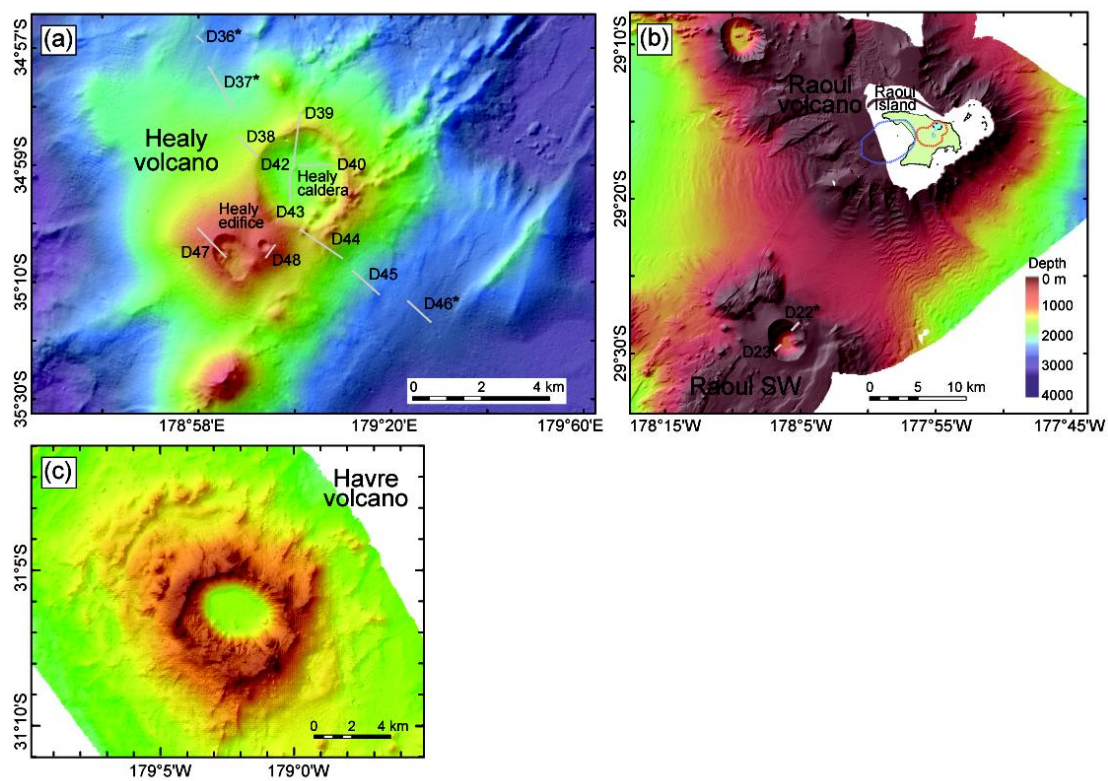


Fig. 2

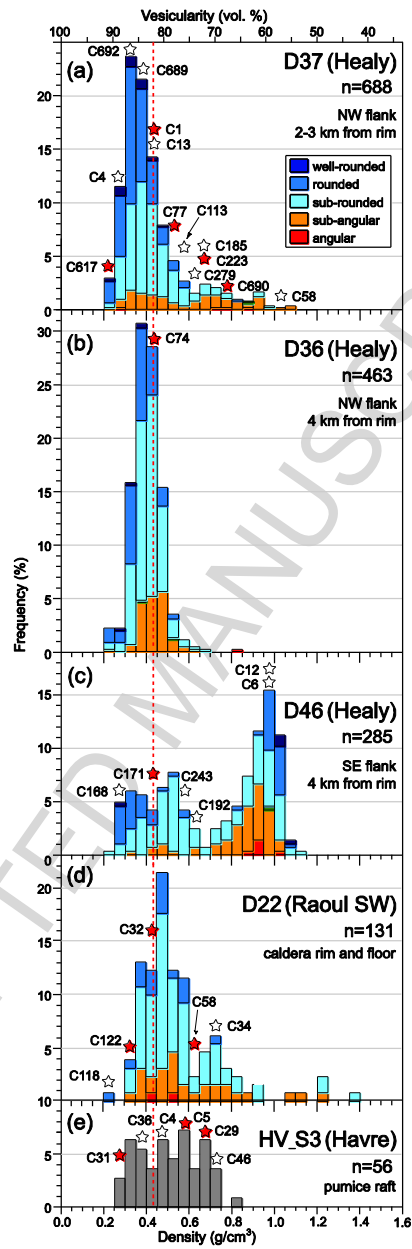


Fig. 3

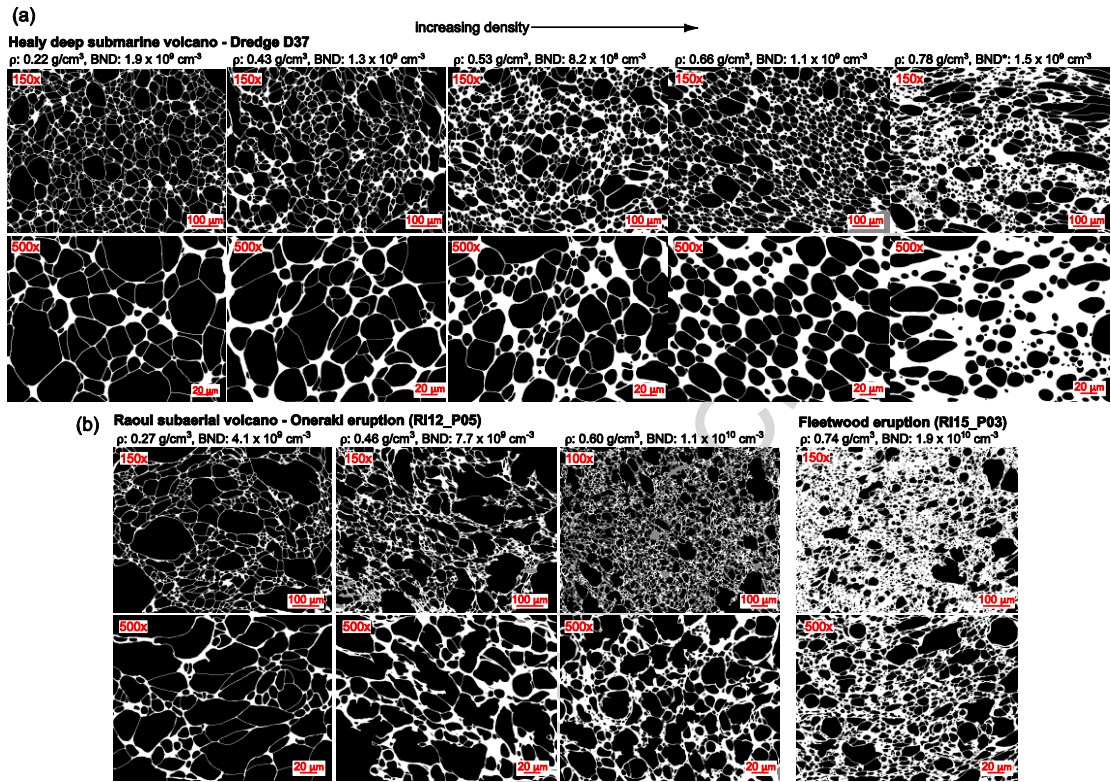


Fig. 4

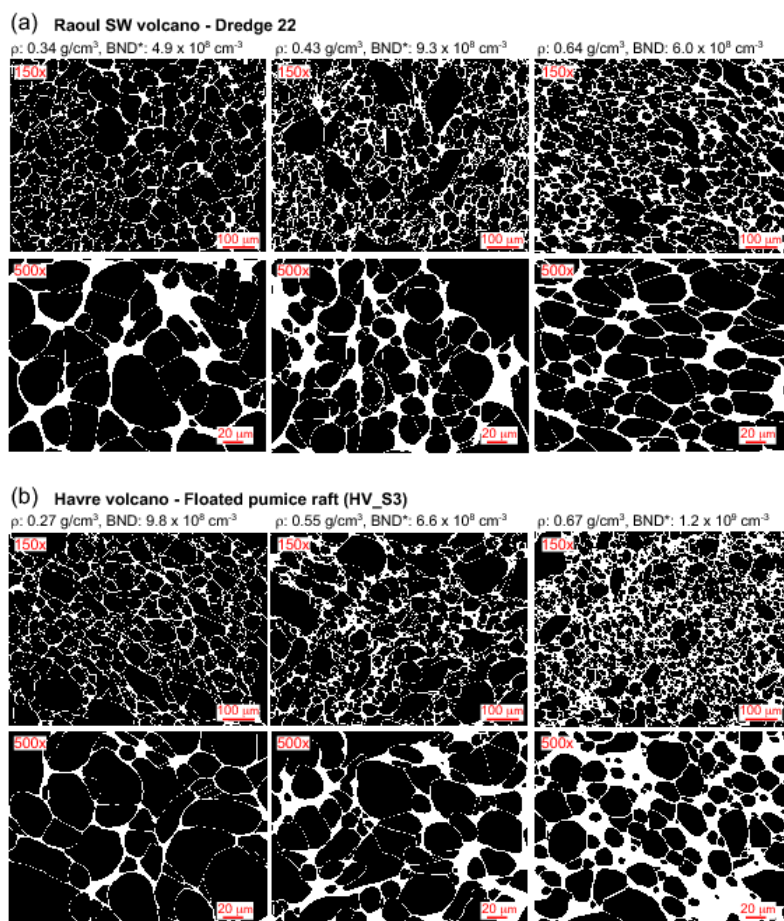


Fig 5.

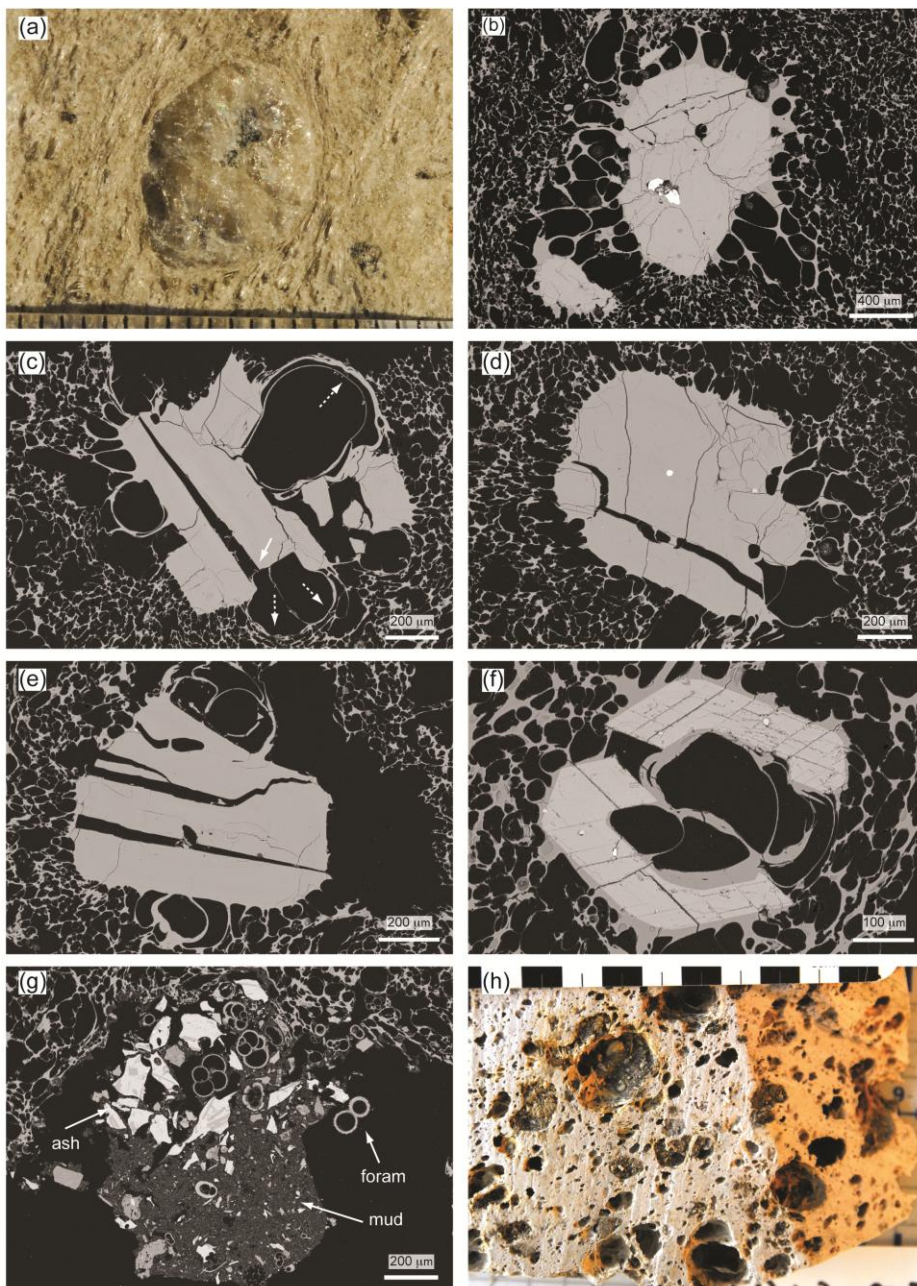


Fig. 6

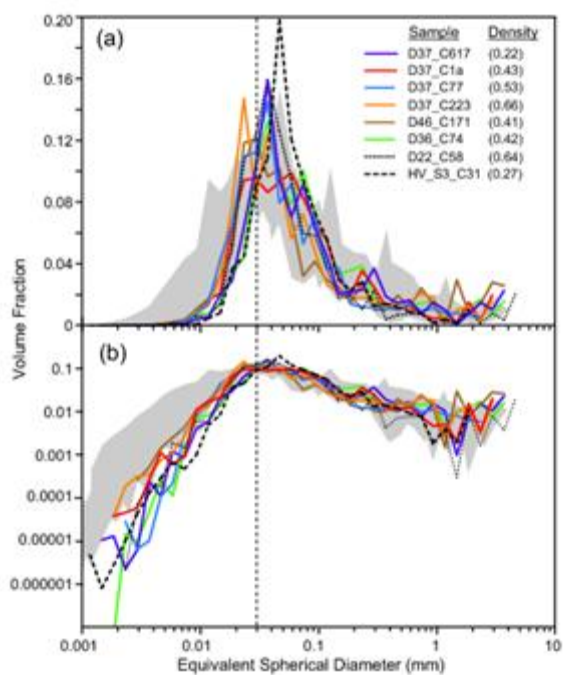


Fig. 7

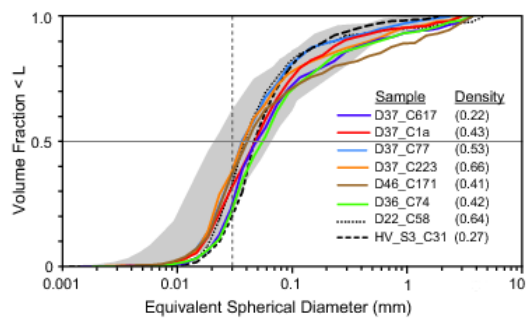


Fig. 8

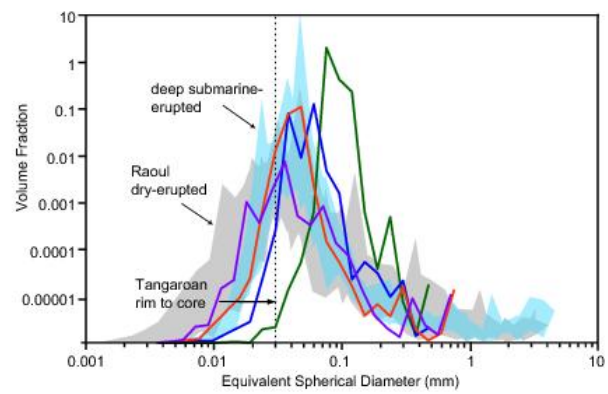


Fig. 9

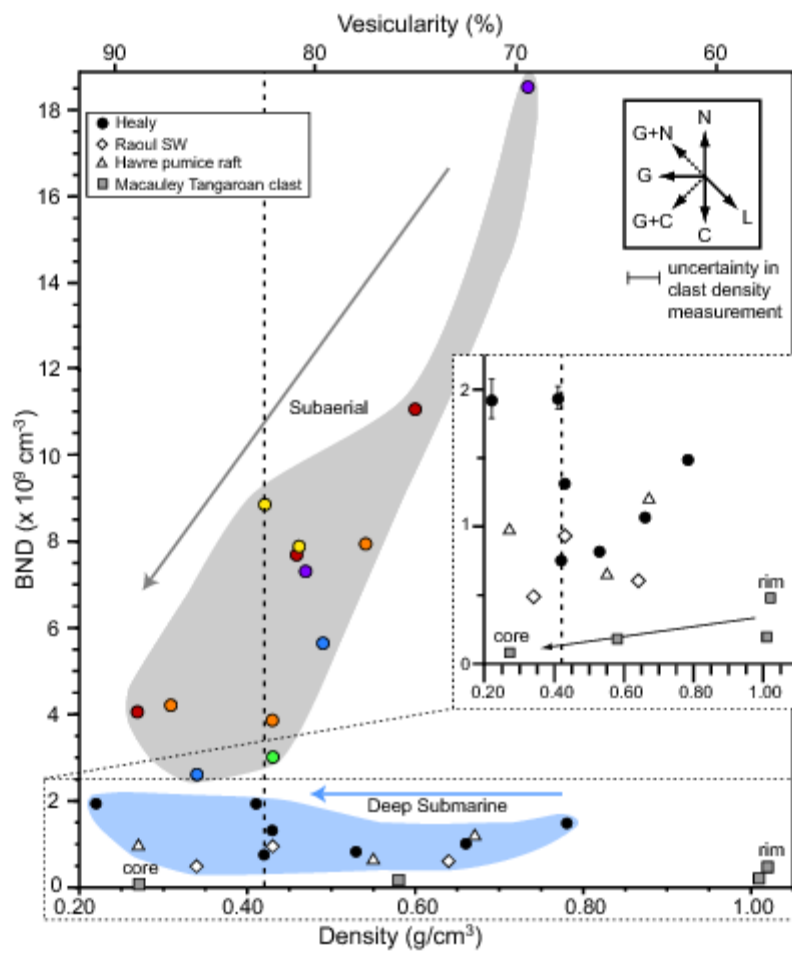


Fig. 10

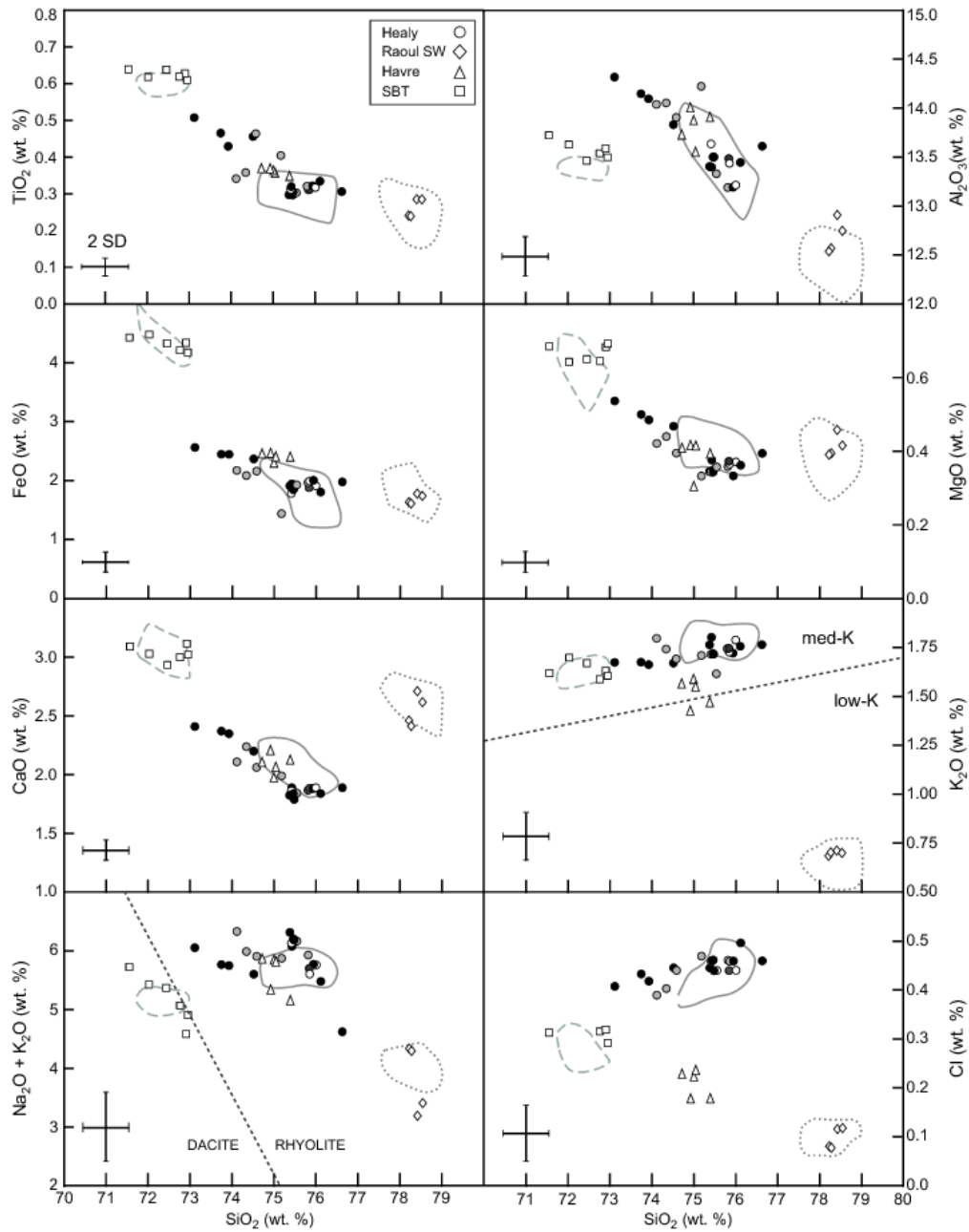


Fig. 11

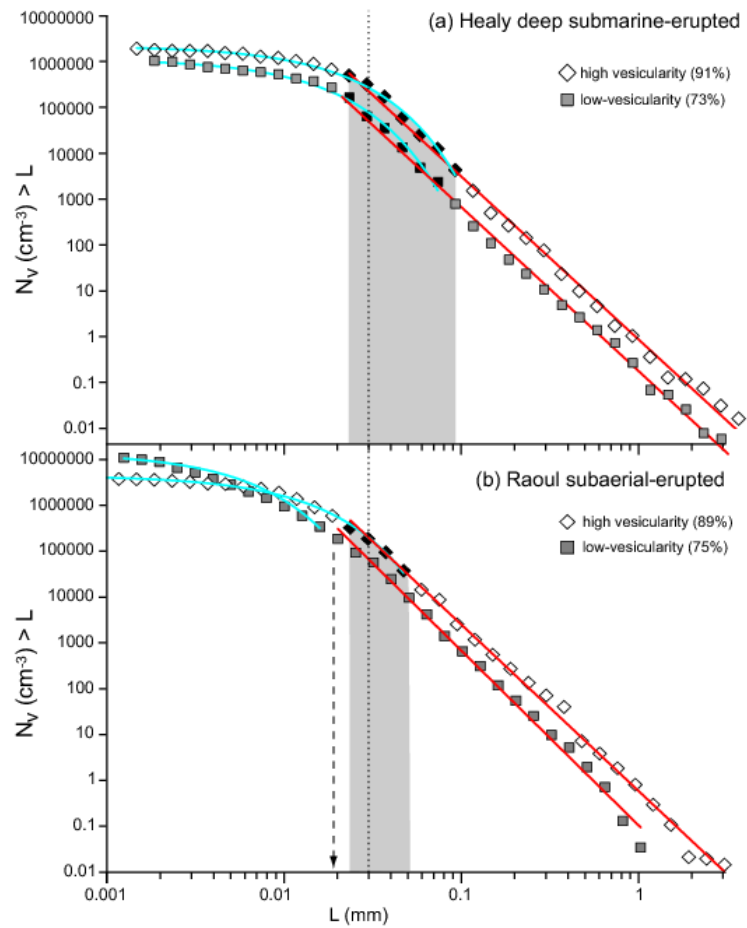


Fig. 12

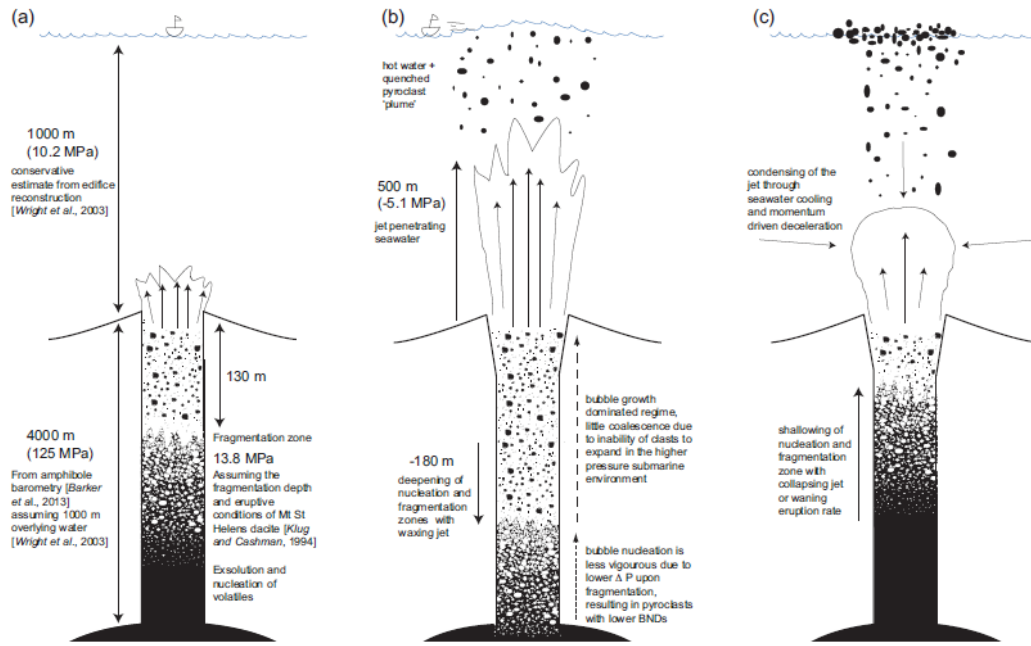


Fig. 13

ACCEPTED

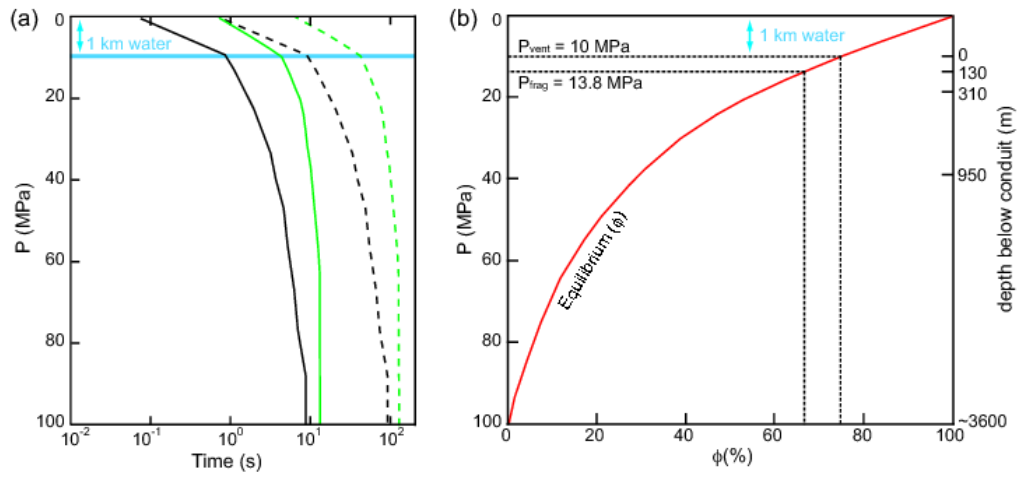


Fig. 14

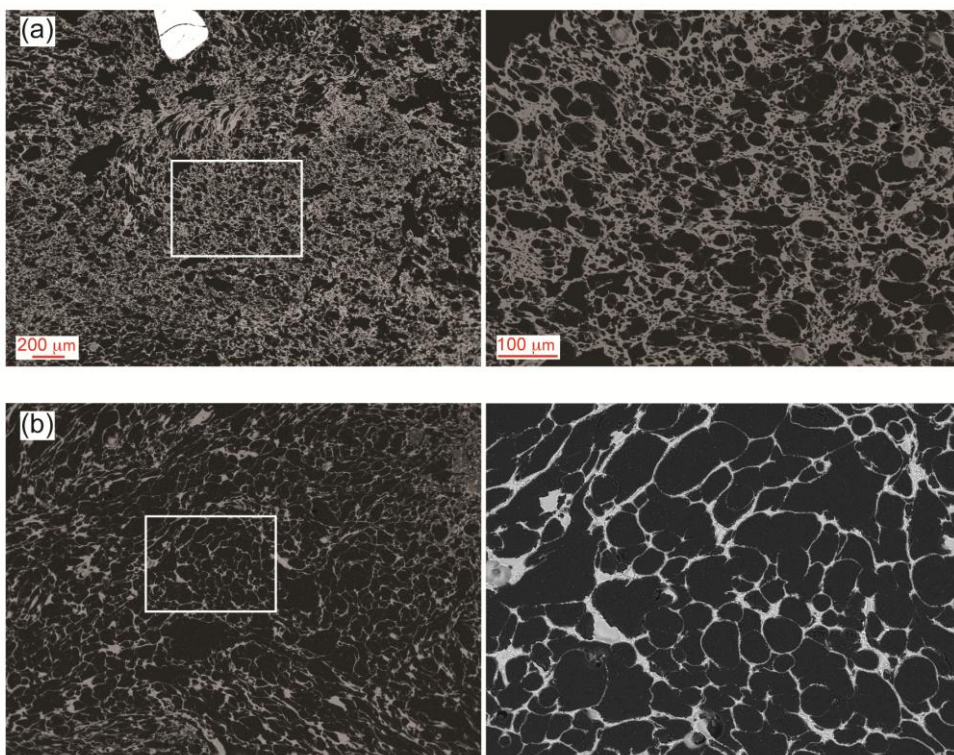


Fig. 15

Table 1. Vesicularity Data

Sample	Density (g/cm ³)	Vesic ^a (%)	BND ^b (cm ⁻³)	BND _{corr} ^c (cm ⁻³)	Largest exp bubble ^d (μm)	Exp R ²	Smallest power law bubble ^e (μm)	Power law exponent	Power law R ²	Mean diameter ^f (μm)	Bubbles counted
Healy volcano											
D36_C74	0.42	82.7	1.3E+08	7.5E+08	74	0.994	29	-3.6	0.997	56	974
D37_C617	0.22	91.0	1.7E+08	1.9E+09	93	0.993	23	-3.5	0.996	49	861
D37_C1	0.43	82.0	2.3E+08	1.3E+09	58	0.994	23	-3.7	0.996	48	1132
D37_C77	0.53	77.7	1.8E+08	8.2E+08	74	0.990	23	-3.8	0.998	37	1105
D37_C223	0.66	72.7	2.9E+08	1.1E+09	74	0.991	23	-3.6	0.997	37	1056
D37_C690*	0.78	67.4	4.9E+08	1.5E+09	-	-	-	-	-	-	1071
D46_C171	0.41	83.1	3.3E+08	1.9E+09	74	0.997	29	-3.4	0.994	41	1242
Raoul SW volcano											
D22_C122*	0.34	85.8	6.9E+07	4.9E+08	-	-	-	-	-	-	312
D22_C32*	0.43	82.2	1.7E+08	9.3E+08	-	-	-	-	-	-	608
D22_C58	0.64	73.4	1.6E+08	6.0E+08	74	0.994	29	-3.8	0.991	39	915
Havre volcano floated pumice raft											
HV_S3_C31	0.27	88.8	1.1E+08	9.8E+08	93	0.995	37	-4.0	0.997	52	818
HV_S3_C5*	0.55	76.9	1.5E+08	6.6E+08	-	-	-	-	-	-	553
HV_S3_C26	0.67	72.1	3.4E+08	1.2E+09	-	-	-	-	-	-	717

^a Vesicularity calculated from density assuming a dense rock equivalent of 2.4 g/cm³

^b Uncorrected bubble number density using a 5-pixel cut off

^c Bubble number density corrected for vesicle and phenocryst (>30 μm) content using a 5-pixel cut off

^d Largest size bin containing bubbles of exponential distribution

^e Smallest size bin containing bubbles of power law distribution

^f Bubble size at 50% cumulative volume fraction

* Obtained from 500x images only; exclusion of bubbles in higher magnification images does not affect the BND_{corr} values outside the uncertainty of the density measurement. See text and Rotella et al. (2014) for further discussion.

Table 2. Average major element glass concentrations for pyroclasts analysed by electron microprobe

Sample	D22_C32	D22_C34	D22_C58	D22_C118	D36_C74	D37_C13	D37_C185	D37_C1	D37_C223	D37_C279	D37_C4	D37_C58	D37_C617	D37_C689	D37_C77
Volcano	Raoul SW	Raoul SW	Raoul SW	Raoul SW	Healy	Healy	Healy	Healy	Healy	Healy	Healy	Healy	Healy	Healy	Healy
SiO ₂	78.54	78.28	78.42	78.22	75.84	74.52	76.05	75.94	75.38	75.48	73.75	73.93	73.12	75.43	75.46
TiO ₂	0.285	0.240	0.286	0.243	0.311	0.456	0.329	0.322	0.297	0.305	0.466	0.430	0.508	0.319	0.297
Al ₂ O ₃	12.75	12.57	12.91	12.54	13.48	13.83	13.45	13.19	13.40	13.50	14.15	14.09	14.32	13.40	13.50
FeO	1.74	1.61	1.78	1.64	1.89	2.37	1.91	2.01	1.91	1.87	2.45	2.45	2.57	1.95	1.85
MnO	0.121	0.111	0.129	0.090	0.094	0.102	0.099	0.086	0.070	0.078	0.117	0.094	0.079	0.100	0.044
MgO	0.417	0.395	0.459	0.392	0.374	0.469	0.374	0.334	0.346	0.351	0.501	0.486	0.538	0.377	0.345
CaO	2.62	2.42	2.71	2.46	1.87	2.20	1.86	1.88	1.82	1.79	2.37	2.35	2.41	1.89	1.83
Na ₂ O	2.71	3.60	2.48	3.65	3.95	3.93	3.71	4.05	4.55	4.47	4.09	4.09	4.38	4.28	4.49
K ₂ O	0.699	0.701	0.711	0.684	1.746	1.672	1.733	1.722	1.765	1.718	1.676	1.664	1.675	1.803	1.718
Cl	0.118	0.078	0.116	0.081	0.440	0.446	0.492	0.460	0.446	0.440	0.434	0.419	0.408	0.461	0.462
Total	96.66	99.24	98.08	99.42	100.49	99.81	99.86	99.54	100.74	100.32	100.72	99.01	100.94	101.92	100.37
n	16	16	5	12	18	38	2	5	18	15	9	7	5	14	15

Sample	D44_C111	D44_C118	D44_C22	D46_C6	D46_C12	D46_C168	D46_C171	D46_C192	D46_C243	HV_S3_C5	HV_S3_C29	HV_S3_C31	HV_S3_C36	HV_S3_C46	SBT
Volcano	Healy	Healy	Healy	Healy	Healy	Healy	Healy	Healy	Healy	Havre	Havre	Havre	Havre	Havre	Macuauley
SiO ₂	75.42	76.00	75.85	75.18	74.59	74.35	75.81	74.12	75.55	75.39	75.05	74.92	74.72	75.00	72.43
TiO ₂	0.311	0.317	0.312	0.405	0.464	0.358	0.321	0.342	0.303	0.349	0.357	0.369	0.371	0.364	0.626
Al ₂ O ₃	13.63	13.21	13.44	14.22	13.90	14.05	13.19	14.04	13.33	13.91	13.55	14.00	13.73	13.87	13.58
FeO	1.79	1.91	2.00	1.44	2.16	2.09	1.97	2.18	1.93	2.41	2.41	2.47	2.46	2.31	4.333
MnO	0.051	0.084	0.094	0.078	0.072	0.082	0.092	0.072	0.079	0.101	0.102	0.097	0.106	0.096	0.141
MgO	0.344	0.372	0.364	0.334	0.396	0.441	0.359	0.422	0.358	0.394	0.414	0.417	0.409	0.305	0.669
CaO	1.86	1.89	1.88	1.99	2.06	2.24	1.87	2.11	1.84	2.12	2.06	2.21	2.11	1.98	3.04
Na ₂ O	4.42	3.98	3.88	4.17	4.22	4.25	4.18	4.54	4.55	3.68	4.27	3.91	4.31	4.27	3.55
K ₂ O	1.717	1.789	1.728	1.710	1.693	1.743	1.746	1.798	1.616	1.468	1.548	1.426	1.565	1.587	1.634
Cl	0.459	0.441	0.460	0.470	0.441	0.404	0.461	0.390	0.441	0.178	0.237	0.177	0.229	0.224	0.310
Total	101.11	101.62	98.98	98.41	98.64	101.02	101.52	100.65	100.31	101.53	100.52	101.71	101.57	100.72	98.89
n	6	5	16	2	13	10	23	17	14	3	13	4	12	11	*

Oxide abundances given in wt.% and normalised to 100% on a volatile free basis, with original analytical totals given. n refers to number of glass analyses per sample. *Sandy Bay Tephra (SBT) data are from 83 analyses of 6 clasts sampled within stratigraphy from 3 locations on Macuauley Island.

Table 3. Representative major and trace element whole-rock compositions of Kermadec pumices

Sample	D38_PC06	D39_PC05	D22_PC02	D23_PC02	51-1	S1
Volcano	Healy	Healy	Raoul SW	Raoul SW	Havre	Havre
Location	NW flank / rim	N rim / wall	NE rim / wall	SW floor / wall	SE flank	Pumice raft
SiO ₂	69.65	72.67	74.12	74.16	72.00	72.11
TiO ₂	0.481	0.411	0.395	0.399	0.437	0.458
Al ₂ O ₃	14.69	14.01	13.70	13.69	14.13	13.99
Fe ₂ O ₃	3.72	2.81	2.60	2.58	3.20	3.35
MnO	0.117	0.112	0.119	0.121	0.116	0.116
MgO	1.265	0.618	0.646	0.699	0.656	0.639
CaO	3.72	2.54	3.64	3.62	2.68	2.67
Na ₂ O	4.74	5.00	4.02	3.97	5.23	5.15
K ₂ O	1.504	1.754	0.668	0.671	1.464	1.439
P ₂ O ₅	0.106	0.074	0.090	0.095	0.084	0.083
LOI	1.48	1.11	2.99	3.48	1.23	1.08
Total	100.15	99.70	99.97	101.71	99.99	99.46
Sc	12.6	8.3	17.1	16.7	11.5	11.3
V	51.0	14.1	13.3	12.7	14.8	14.9
Cr	6.75	2.20	1.62	0.90	3.94	11.48
Ni	3.37	0.61	0.89	1.41	0.30	0.45
Cu	20.16	7.39	6.37	8.27	8.56	9.96
Zn	51.8	60.8	72.3	77.5	68.4	65.8
Ga	16.5	15.8	14.8	14.7	17.7	16.4
Rb	24.65	29.62	10.22	10.39	31.46	28.78
Sr	220	203	167	169	149	131
Y	38.8	41.7	38.9	38.6	48.9	44.6
Zr	162.5	178.9	81.9	82.9	203.9	184.8
Nb	2.996	3.396	0.708	0.725	2.638	2.392
Mo	1.65	1.09	1.87	1.86	2.19	2.53
Cs	0.732	0.754	0.838	0.841	1.472	1.354
Ba	788	915	225	231	475	430
La	13.04	14.17	5.08	5.11	13.66	12.18
Ce	29.97	32.34	13.49	13.59	34.30	30.54
Pr	4.27	4.52	2.19	2.21	5.05	4.40
Nd	18.93	20.26	11.27	11.46	23.34	20.57
Sm	4.91	5.16	3.73	3.75	6.15	5.41
Eu	1.44	1.47	1.20	1.20	1.70	1.49
Gd	5.43	5.58	4.70	4.86	6.82	5.79
Tb	0.926	0.968	0.857	0.878	1.135	0.976
Dy	6.16	6.45	6.06	6.17	7.76	6.86
Ho	1.32	1.40	1.34	1.37	1.70	1.49
Er	4.08	4.24	4.06	4.14	5.06	4.57
Tm	0.634	0.661	0.639	0.634	0.787	0.696
Yb	4.32	4.67	4.26	4.37	5.29	4.53
Lu	0.659	0.723	0.659	0.665	0.811	0.699
Hf	4.34	4.69	2.59	2.64	5.49	4.87
Ta	0.198	0.264	0.052	0.054	0.209	0.188
W	0.253	0.506	0.244	0.261	0.549	0.592
Pb	3.81	4.73	3.68	3.72	7.41	6.65
Th	2.352	2.711	0.697	0.722	3.152	2.653
U	0.692	0.805	0.277	0.294	0.952	0.841

Healy and Raoul SW data are for the most and least evolved samples from Barker et al. (2013). Havre sample 51-1 is from Wright et al. (2006). Oxide abundances given in wt.% and normalised to 100% on a volatile free basis, with original LOI values and analytical totals given. LOI is weight loss on ignition at 1000°C for ~1 hour. Trace elements analysed by solution ICP-MS with concentrations given in

Highlights

1. We examined bubble size distributions for deep submarine-erupted silicic pumice
2. Deep submarine pumice has markedly different microtextures to subaerial pumice
3. Bubble number densities are lower for deep submarine- vs subaerial-erupted pumice
4. Higher pressure suppresses rapid magma acceleration, coalescence and permeability
5. Microtextures allow fingerprinting subaerial/submarine pumice in ancient deposits

ACCEPTED MANUSCRIPT